T H E U N I V E R S I T Y O F M I C H I G A N

COLLEGE OF ENGINEERING
Department of Electrical Engineering
Space Physics Research Laboratory

Sounding Rocket Flight Report

NASA 18.49 THERMOSPHERE PROBE EXPERIMENT

Prepared on behalf of the project by

R. W. Simmons

ORA Project 07065

under contract with:

NATIONAL AERONAUTICS AND SPACE ADMINISTRATION
GODDARD SPACE FLIGHT CENTER
CONTRACT NO. NAS 5-9113
GREENBELT, MARYLAND

administered through:

OFFICE OF RESEARCH ADMINISTRATION ANN ARBOR

May 1969

TABLE OF CONTENTS

ACKNOWLEDGMENTS

The launching of NASA 18.49 was one of a series conducted during an expedition to Puerto Rico. The launch facilities at Mar Chiquita were set up and operated by personnel from NASA, Wallops Station, under the direction of Mr. Robert Long. The launchings were coordinated with the Arecibo Ionosphere Observatory under the direction of Dr. H. C. Carlson.

The Thermosphere Probe launchings were conducted under Contract No. NAS 5-9113 as part of a cooperative undertaking of the Goddard Space Flight Center and the Space Physics Research Laboratory of The University of Michigan. Over one hundred persons contributed to the success of the NASA 18.49 Thermosphere Probe Experiment. Some of the personnel with specific responsibilities are listed below.

Goddard Space Flight Center

Spencer, N. W.	Project Director
Brace, L. H.	Scientist
Mahajan, K. K.	Scientist

Space Physics Research Laboratory

Carignan, G. R.	Laboratory Director
Taeusch, D. R.	Associate Laboratory Director
Caldwell, J. R.	Electronics Engineer
Campbell, B. J.	Design Draftsman
Crosby, D. F.	Electron Temperature Probe Engineer
Freed, P. L.	Head Technician
Kartlick, W. G.	Omegatron Technician
Kimble, R. G.	Telemetry Technician
Maurer, J. C.	Payload Engineer
McCormick, D. L.	Machinist
Niemann, H. B.	Neutral Particle Scientist
Pate, R. W.	Omegatron Engineer
Poole, G. T.	Head Programmer

LIST OF ILLUSTRATIONS

LIST OF ILLUSTRATIONS (Concluded)

1. INTRODUCTION

The results of the launching of NASA 18.49, a Nike-Tomahawk sounding rocket, are presented and discussed in this report. The payload, a Thermosphere Probe (TP), described by Spencer, Brace, Carignan, Taeusch, and Niemann (1965), was jointly developed by the Space Physics Research Laboratory (SPRL) of The University of Michigan and the Goddard Space Flight Center (GSFC), Laboratory for Atmospheric and Biological Sciences (LABS). The TP is an ejectable instrument package designed for the purpose of studying the variability of the earth's atmospheric parameters in the altitude region between 120 and 350 km. The NASA 18.49 payload included a "first generation" omegatron mass analyzer (Niemann and Kennedy, 1966), an electron temperature probe (Spencer, Brace, and Carignan, 1962), and a lunar position sensor. This complement of instruments permitted the determination of the molecular nitrogen density and temperature and the electron density and temperature in the altitude range of approximately 135 to 275 km over Puerto Rico.

A general description of the payload kinematics, orientation analysis, and the techniques for the reduction and analysis of the data is given by Taeusch, Carignan, Niemann, and Nagy (1965) and Carter (1968). The orientation analysis and the reduction of the nitrogen data were performed at SPRL, and the results are included in this report. Because of improper vehicle performance no electron temperature probe data were available (the probe was destroyed during the abnormal ejection).

2. GENERAL FLIGHT INFORMATION

The general flight information for NASA 18.49 is listed below. Table I gives the flight times and altitudes of significant events which occurred during the flight. Some of these were estimated and are so marked. The others were obtained from the telemetry records and radar trajectory information.

Launch Date:	17 March 1968
Launch Time:	09:28:00.000 GMT, 05:28:00.000 Local
Location:	Puerto Rico
	Latitude: 18°28'57.41" N
	Longitude: 66°26'20.06" W

Apogee Parameters:

Altitude:	311.40 km
Horizontal Velocity:	557.54 m/sec
Flight Time:	287.50 sec

TP Motion:

Tumble Period:	6.53 sec
Roll Rate:	230 deg/sec

TABLE I

TABLE OF EVENTS

(NASA 18.49)

Event	Flight Time (sec)	Altitude (km)
Lift-off	0	0
1st Stage Burnout	3.5 (est.)	1.3 (est.)
2nd Stage Ignition	26.1 (est.)	13.9 (est.)
2nd Stage Burnout	35.1 (est.)	26.1 (est.)
Despin	44.7 (est.)	62.0 (est.)
TP Ejection	46.7	66.0 (est.)
Omegatron Breakoff	77.4	113.4
Omegatron Filament On, M28	79.4	117.2
Peak Altitude	287.50	311.40
L.O.S.	537.0	—

3. LAUNCH VEHICLE

The NASA 18.49 launch vehicle was a two-stage, solid propellant Nike-Tomahawk combination. The first stage, a Hercules M5E1 Nike motor, had an average thrust of 49,000 lb and burned for approximately 3.5 sec. The Nike booster, plus adapter, was 145.2 in. long and 16.5 in. in diameter. Its weight unburned was approximately 1325 lb. The sustainer stage, Thiokol's TE416 Tomahawk motor, provided an average thrust of 11,000 lb and burned for about 9 sec. The Tomahawk, 141.1 in. long and 9 in. in diameter weighed 530 lb unburned. The TP payload, which was 78.4 in. long and weighed 134 lb, including despin and adapter modules, made the total vehicle 364.7 in. long with a gross lift-off weight of 1989 lb. The vehicle is illustrated in Figures 1, 2, 3, and 4.

Due to an apparent malfunction of the second stage firing/despin system, the second stage ignition was delayed 14 sec. This same (or a related) malfunction of the despin device caused an abnormally violent TP ejection which in turn destroyed the electron temperature and density probe, as mentioned earlier. The vehicle reached a summit altitude of 311.40 km at 287.50 sec of flight time.

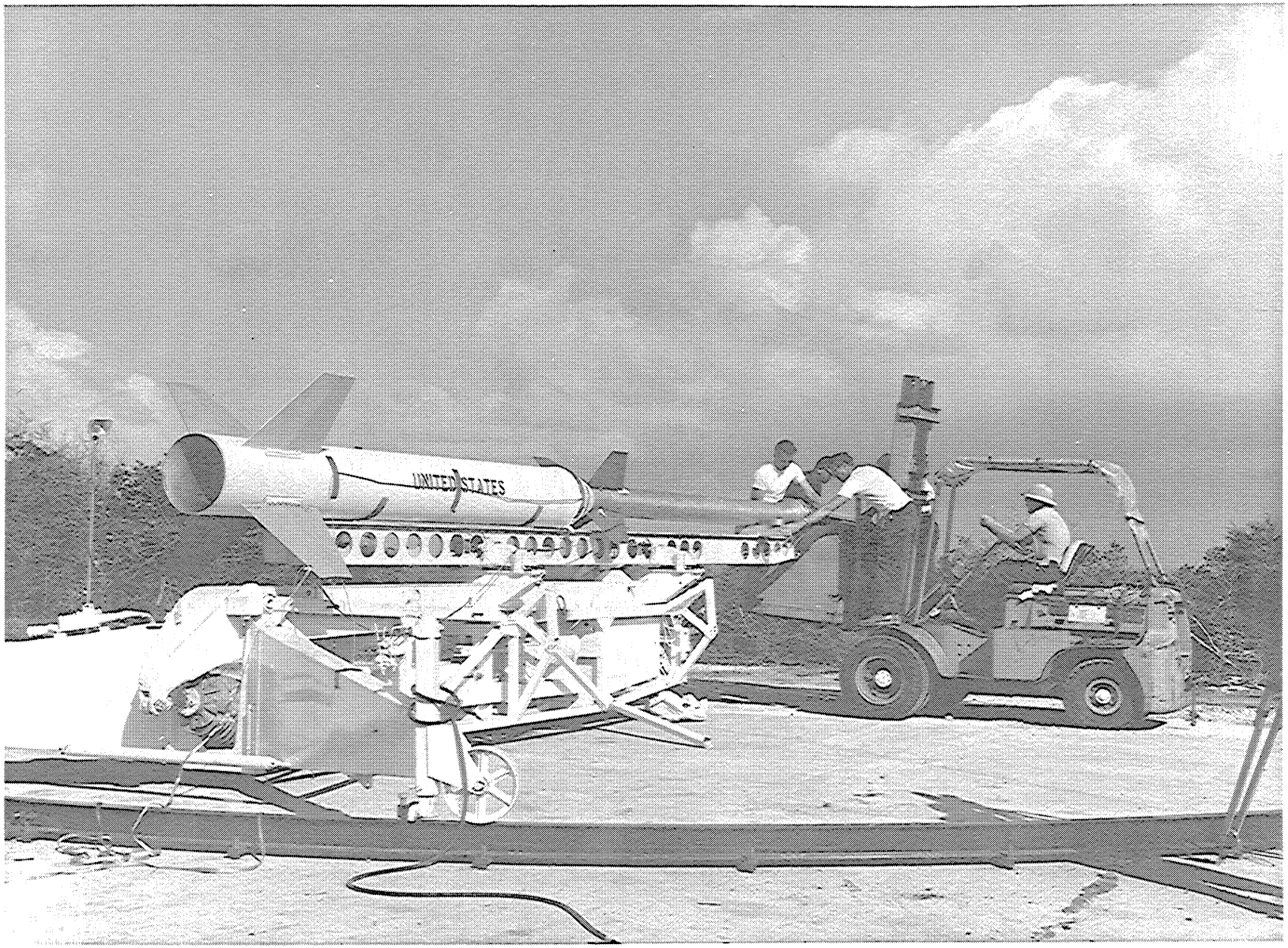

Figure 1. Nike-Tomahawk with thermosphere probe payload.

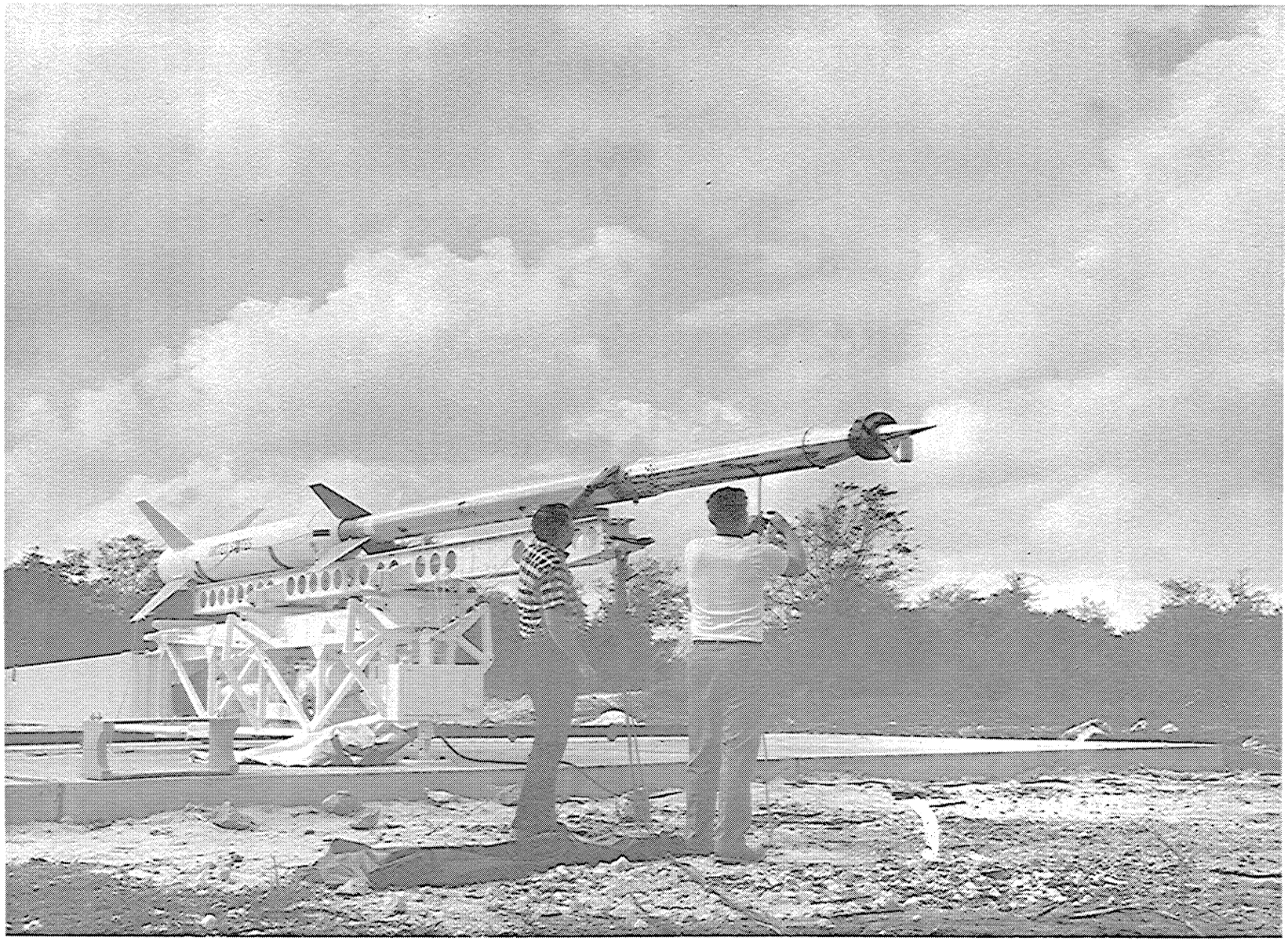

Figure 2. Nike-Tomahawk with thermosphere probe payload.

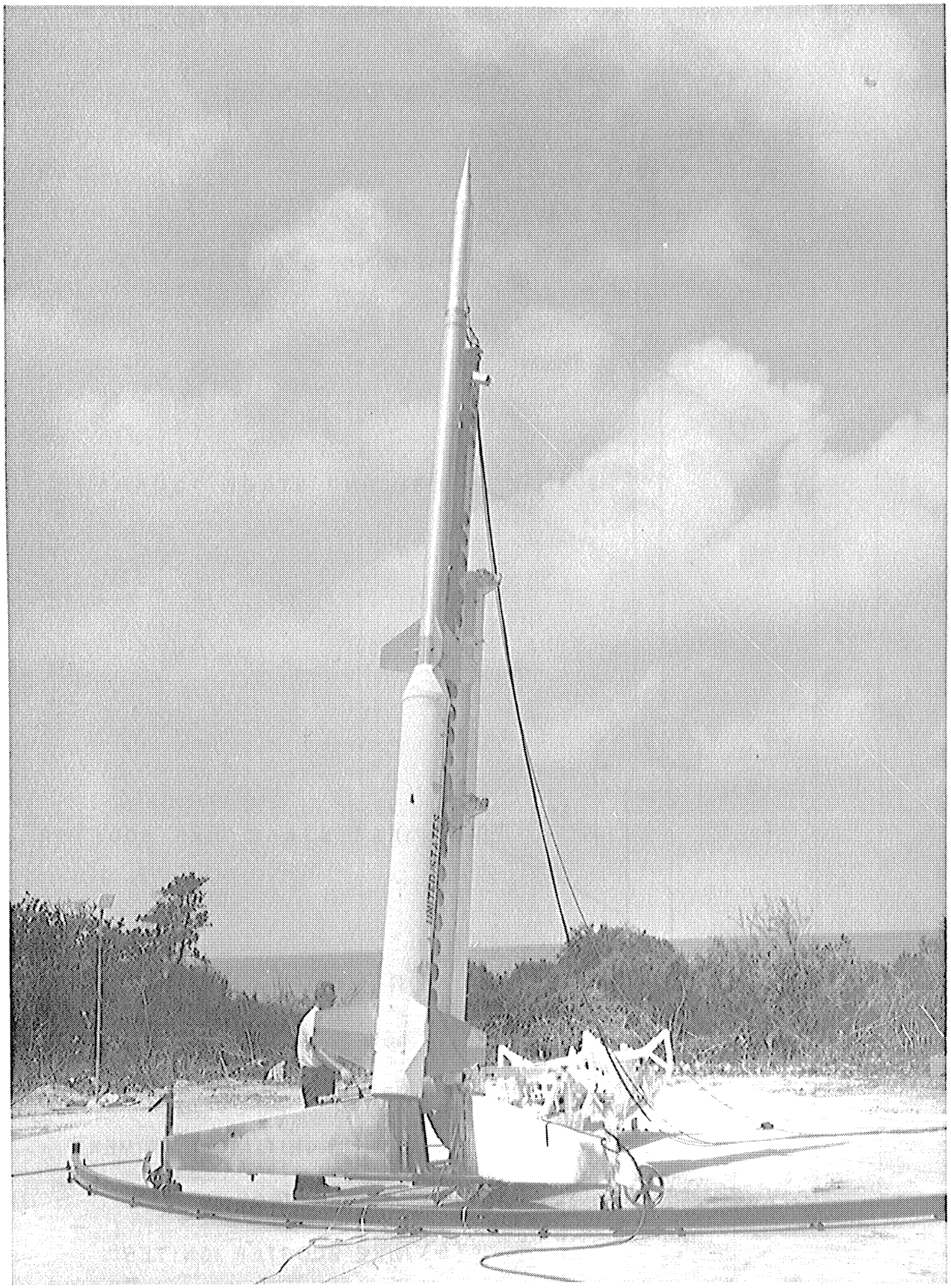

Figure 3. Nike-Tomahawk with thermosphere probe payload.

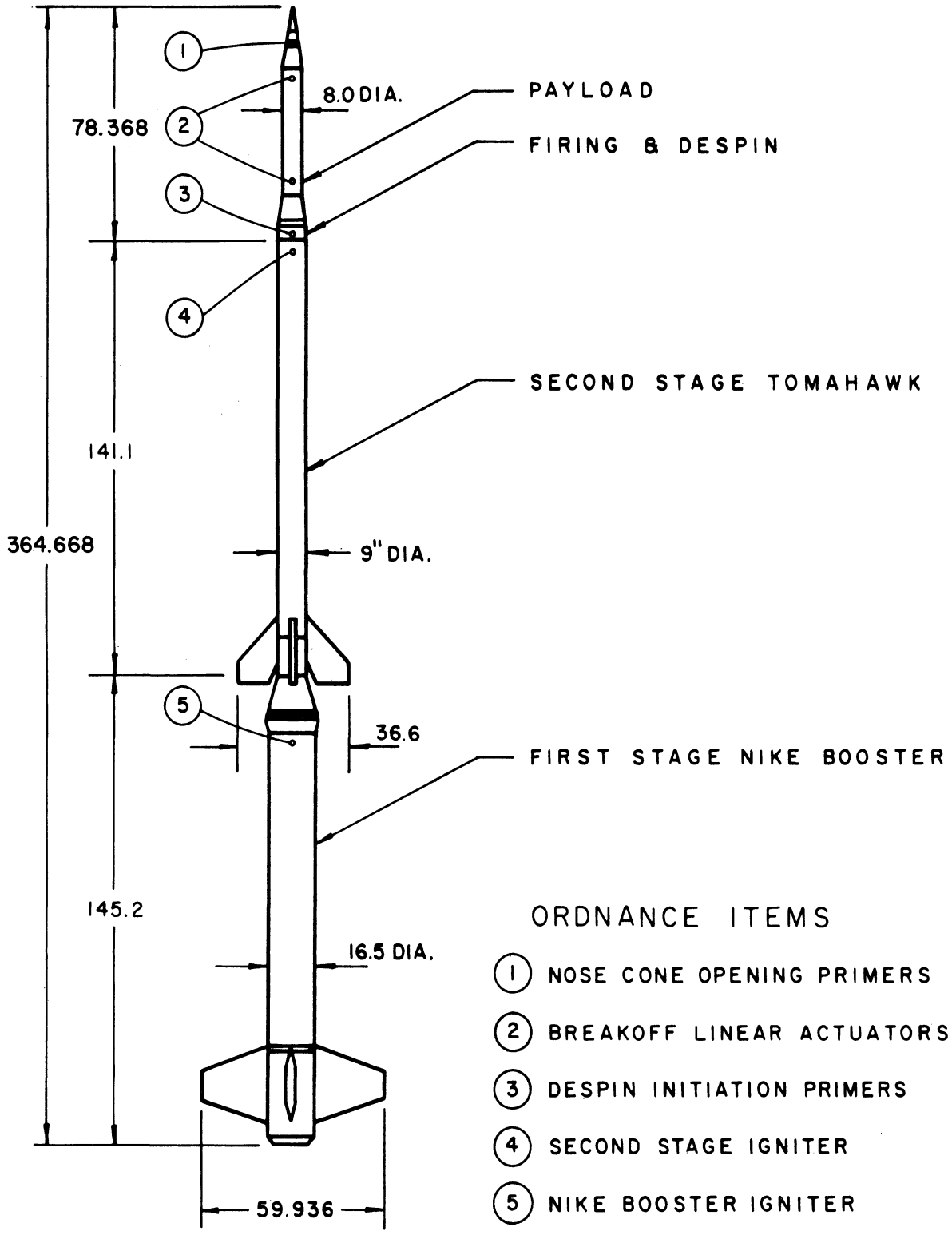

Figure 4. Nike-Tomahawk dimensions.

4. NOSE CONE

A diagram of the NASA 18.49 payload including the nose cone, the despin mechanism, and the adapter section is shown in Figure 5. An assembly drawing of the 8-in. nose cone is given in Figure 6.

The ejection system was designed for a tumble period of 1.5 sec by using a 5.0 lb Neg'ator* force and by limiting the travel of the plunger to 3.0 in. (Carter, 1968). An apparent failure of the despin mechanism caused an abnormal ejection and the design tumble period of 1.5 sec was not achieved. The ejection occurred at 66 km (47 sec after launch) and the resulting tumble period was 6.53 sec. The breakoff device of the omegatron was removed at 113 km (77 sec after launch), and the omegatron filament was turned on approximately 2 sec later.

*Neg'ator is a trade name.

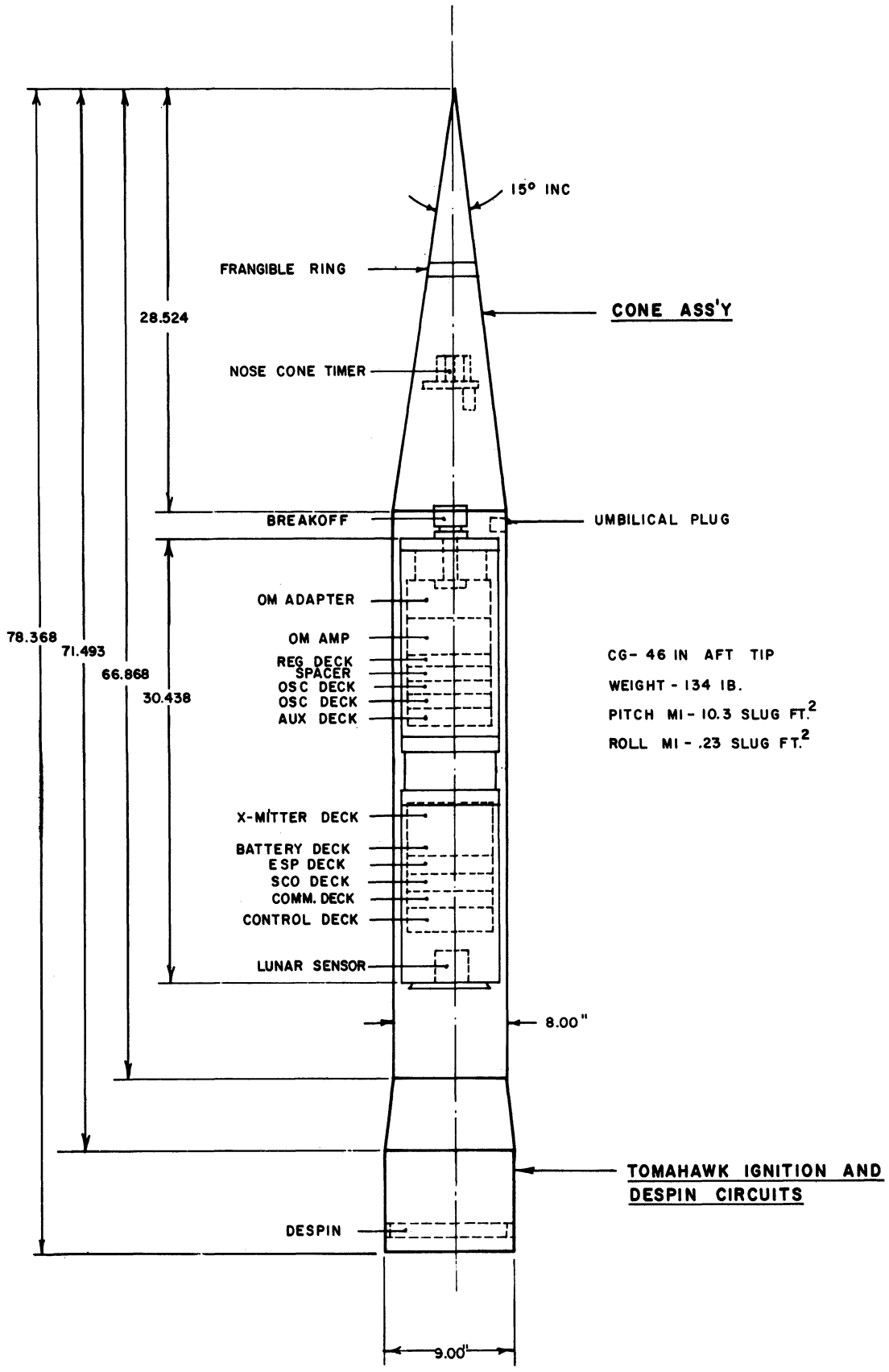

Figure 5. Thermosphere probe instrumentation design.

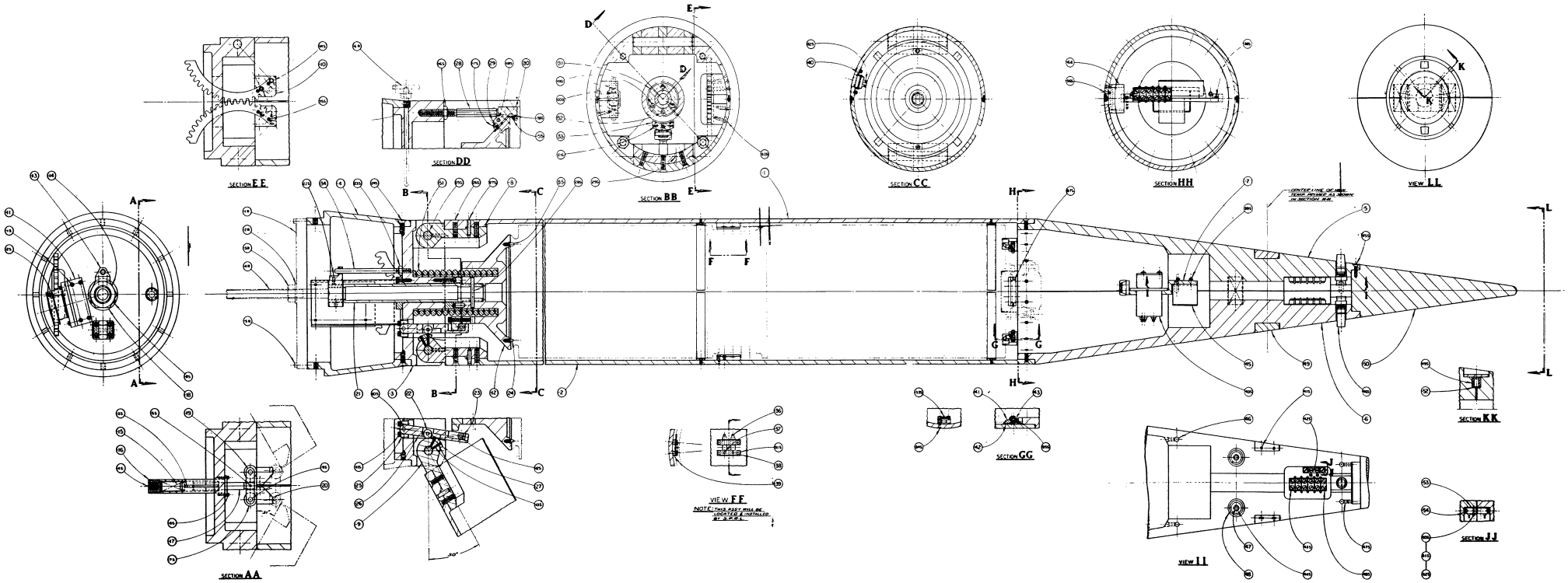

Figure 6. Assembly drawing, 8-in. nose cone.

5. THE THERMOSPHERE PROBE (TP)

The TP used for the NASA 18.49 payload was a cylinder 30.4 in. long and 7.25 in. in diameter which weighed 53.6 lb. The major instrumentation for this payload included an omegatron mass analyzer and an electron temperature probe. Supporting instrumentation included a lunar aspect sensor for use in determining the attitude of the TP. The diagram in Figure 5 shows the location of instrumentation and supporting electronics in the nose cone. Figure 7 is the system block diagram.

5.1. OMEGATRON

The omegatron used in the payload has been described by Niemann and Kennedy (1966). Table II lists the operating parameters of the gauge and associated electronics. The characteristics of the linear electrometer amplifier current detector, used to monitor the omegatron output current, are also listed. The omegatron envelope and breakoff configuration are shown in Figure 8. The calibration of the NASA 18.49 omegatron, performed at SPRL during January 1968, is shown in Figure 9.

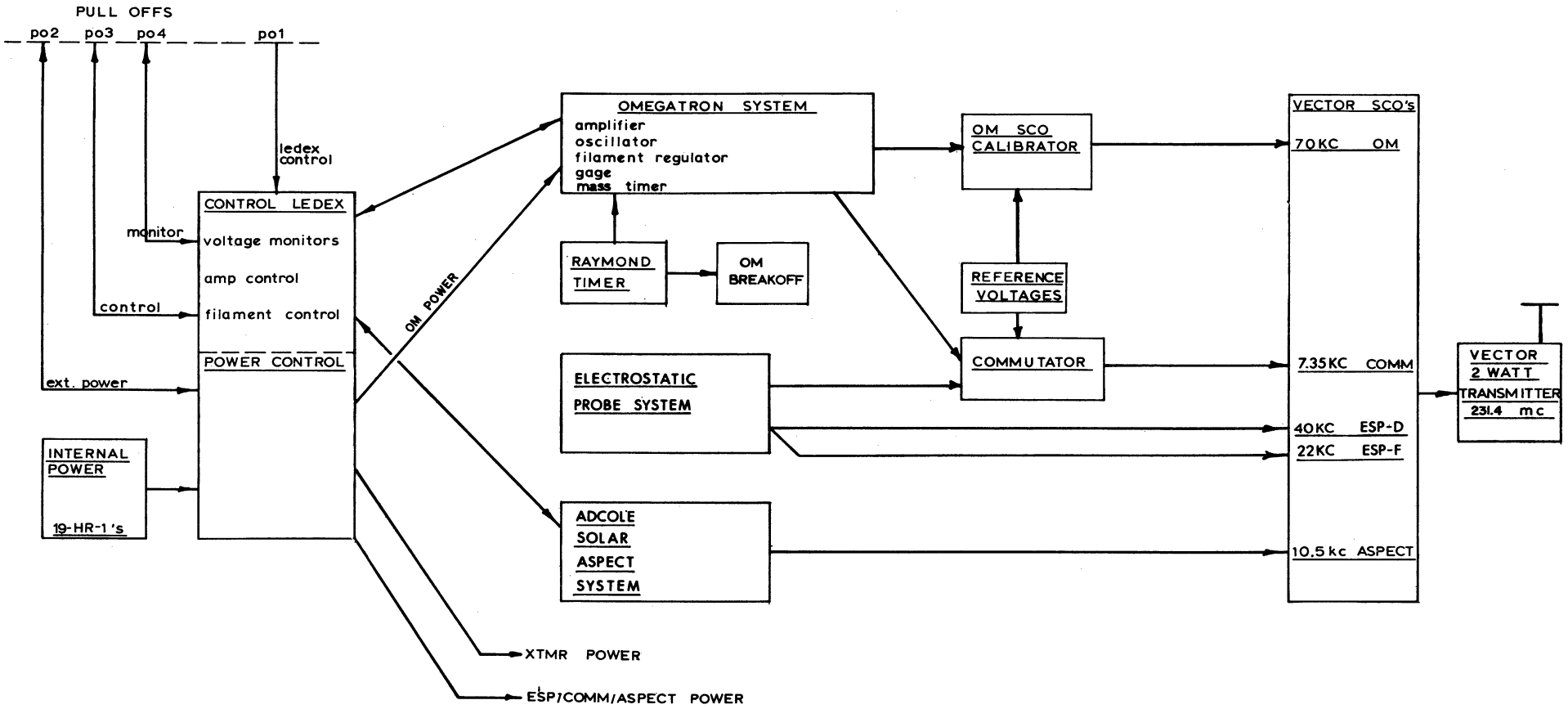

Figure 7. Thermosphere probe system block diagram.

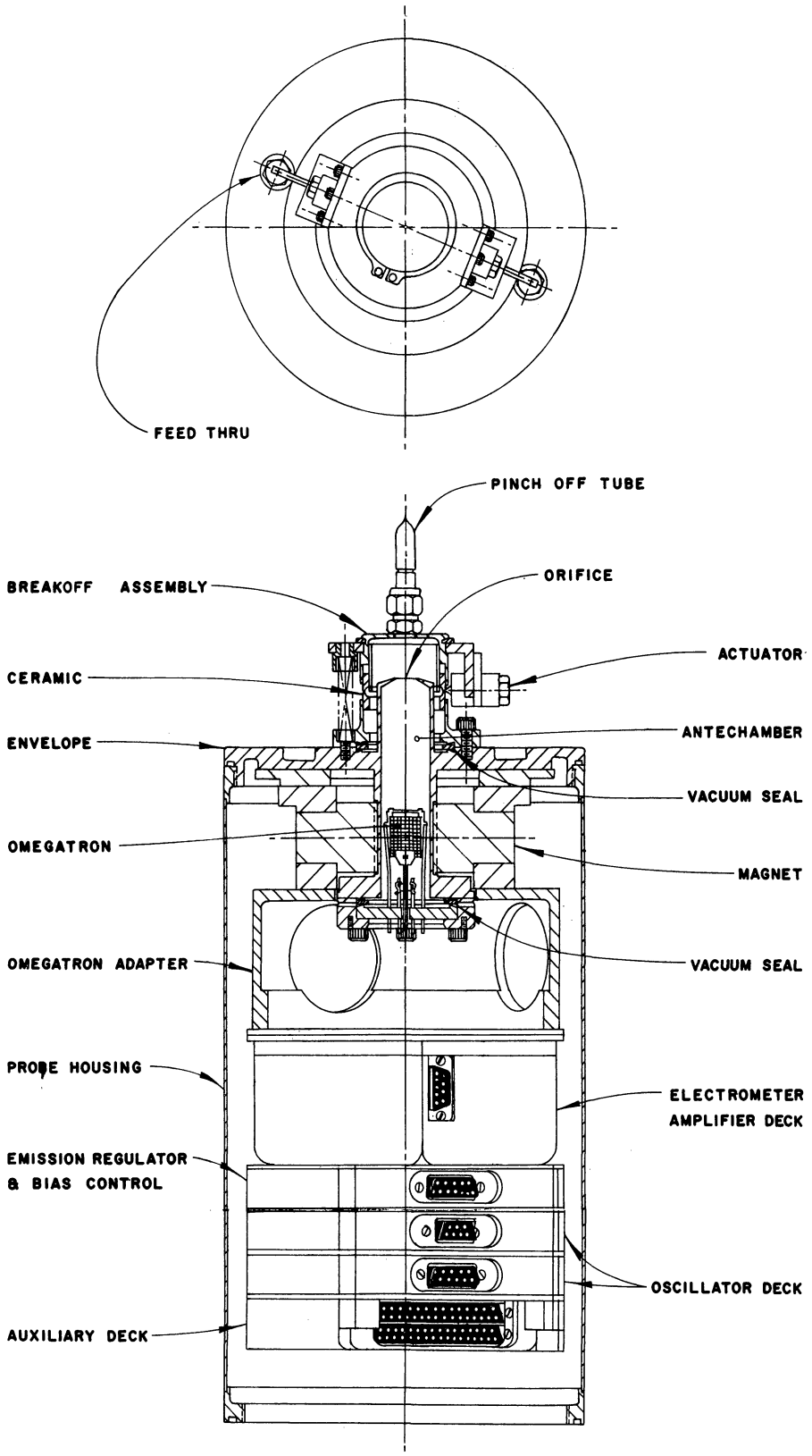

Figure 8. Omegatron I.

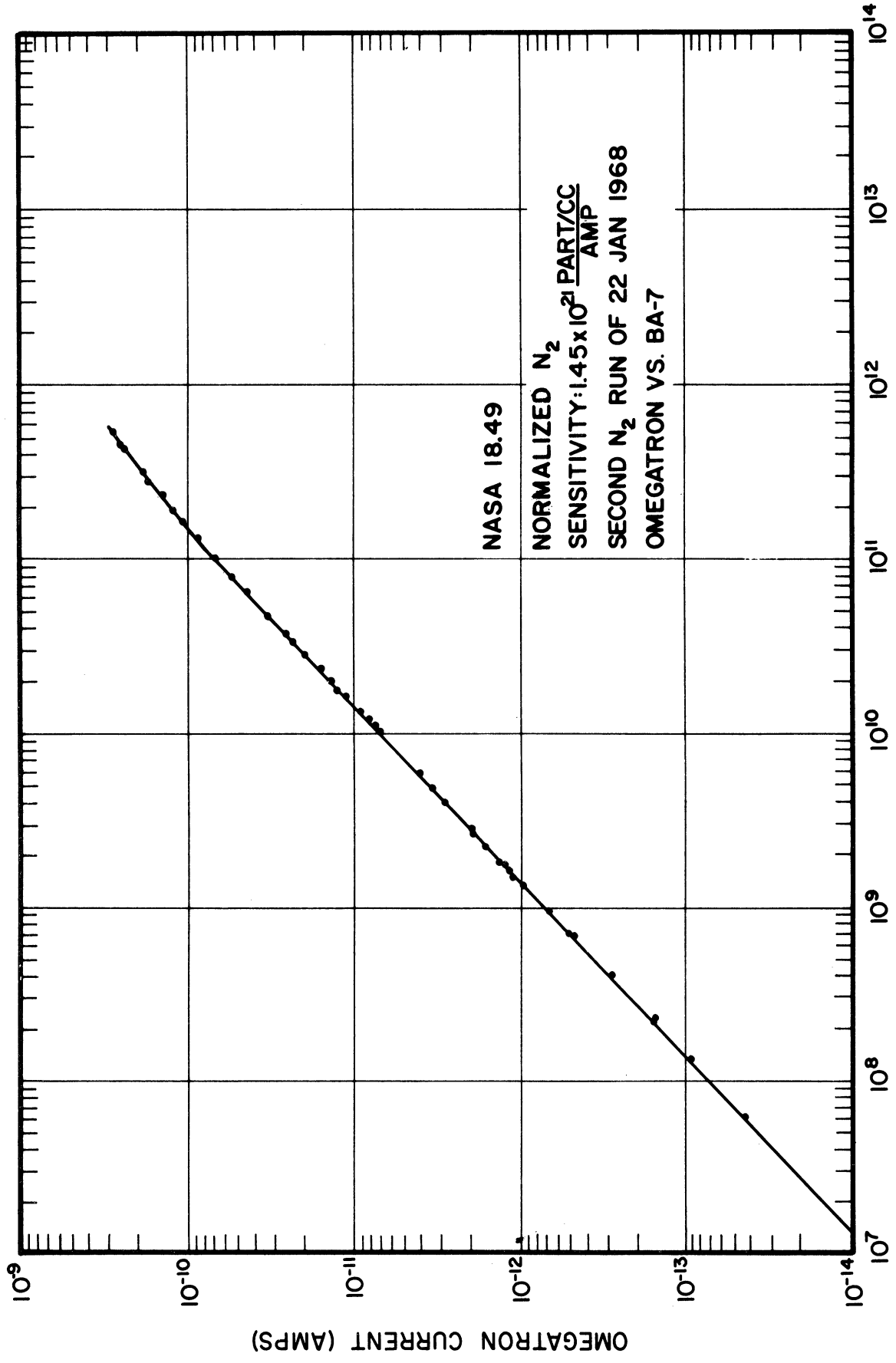

Figure 9. Final calibration of the omegatron.

TABLE II

OMEGATRON DATA

(NASA 18.49)

Omegatron Gauge Parameters	OM I
Beam Current:	2.00 μA
Electron Collector Bias:	73.84 V
Filament Bias:	-90.33 V
Cage Bias:	- 0.21 V
Top Bias:	- 0.60 V
RF Amplitude, Mass 28:	4.00 V_{p-p}
RF Frequency, Mass 28:	144.52 kHz
Monitors	
Filament	
OFF:	0.12 V
ON:	2.85 V
Beam	
OFF:	0.69 V
ON:	3.61 V
Thermistor Pressure ("zero" pressure)	
Filament OFF:	2.03 V
Filament ON:	1.95 V
Bias:	3.85 V
RF:	3.42 V
Calibration	
Normalized N_2 Sensitivity:	2.22 x 10^{-5} A/torr
Maximum Linear Pressure (5%):	7 x 10^{-6} torr

TABLE II (Concluded)

Electrometer Amplifier

OM I

Range	Range Indicator	Range Resistor	Mass 28 ZPV
1	0.0 V	9.119×10^{9} Ω	4.979 V
2	0.7 V	2.479×10^{10} Ω	4.979 V
3	1.4 V	6.738×10^{10} Ω	4.979 V
4	2.1 V	1.832×10^{11} Ω	4.979 V
5	2.8 V	4.979×10^{11} Ω	4.980 V
6	3.5 V	1.353×10^{12} Ω	4.982 V
7	4.2 V	3.679×10^{12} Ω	4.990 V
8	4.9 V	1.000×10^{13} Ω	5.010 V

Miscellaneous

+28 power current all on:	350 mA maximum, 240 mA normal
Preflight gauge pressure (N_2):	5×10^{-6} torr
Magnetic field strength:	2610 gauss

5.2. ELECTRON TEMPERATURE AND DENSITY PROBE

The Electron Temperature and Density Probe (ETDP) for NASA 18.49 consisted of a cylindrical Langmuir probe placed in the plasma and two separate electronics units to measure the current collected by the probe as it is swept through a series of ramp voltages. The cylindrical Langmuir probe is shown in Figure 10 and was made of stainless steel. Although the probe did not work and no ETDP data were obtained (the probe was destroyed during the abnormal ejection), the present report describes the two electronic systems which were to have time-shared the probe.

The System I electronics unit is a new system incorporating many of the design features of the OGO-F-02 satellite experiment. System II is the standard TP electronics package which has been flown many times in the past. The two systems are interconnected so that the sweep times can be synchronized to allow both systems to make measurements on the same probe. While System I is connected to the probe, System II is connected to a precision calibration resistor for in-flight system calibration. At the end of a specified time, the probe is connected to System II and System I is connected to its calibration resistor. This sequence is repeated throughout the flight. Figure 11 shows the interconnection of the two systems and Figure 12 shows the timing and sequencing of the systems.

5.2.1. System I Electronics

The System I electronics unit produces as its outputs a voltage that is proportional to the log of the absolute value of the current collected by the cylindrical Langmuir probe. The system contains a dc-dc convertor, a two-range differential current detector, an absolute value amplifier, a logarithmic amplifier, a ΔV ramp generator with automatic biasing capability, an in-flight calibration system, and various logic, control, and interfacing circuits. The block diagram is shown in Figure 13 and the system specifications are given below:

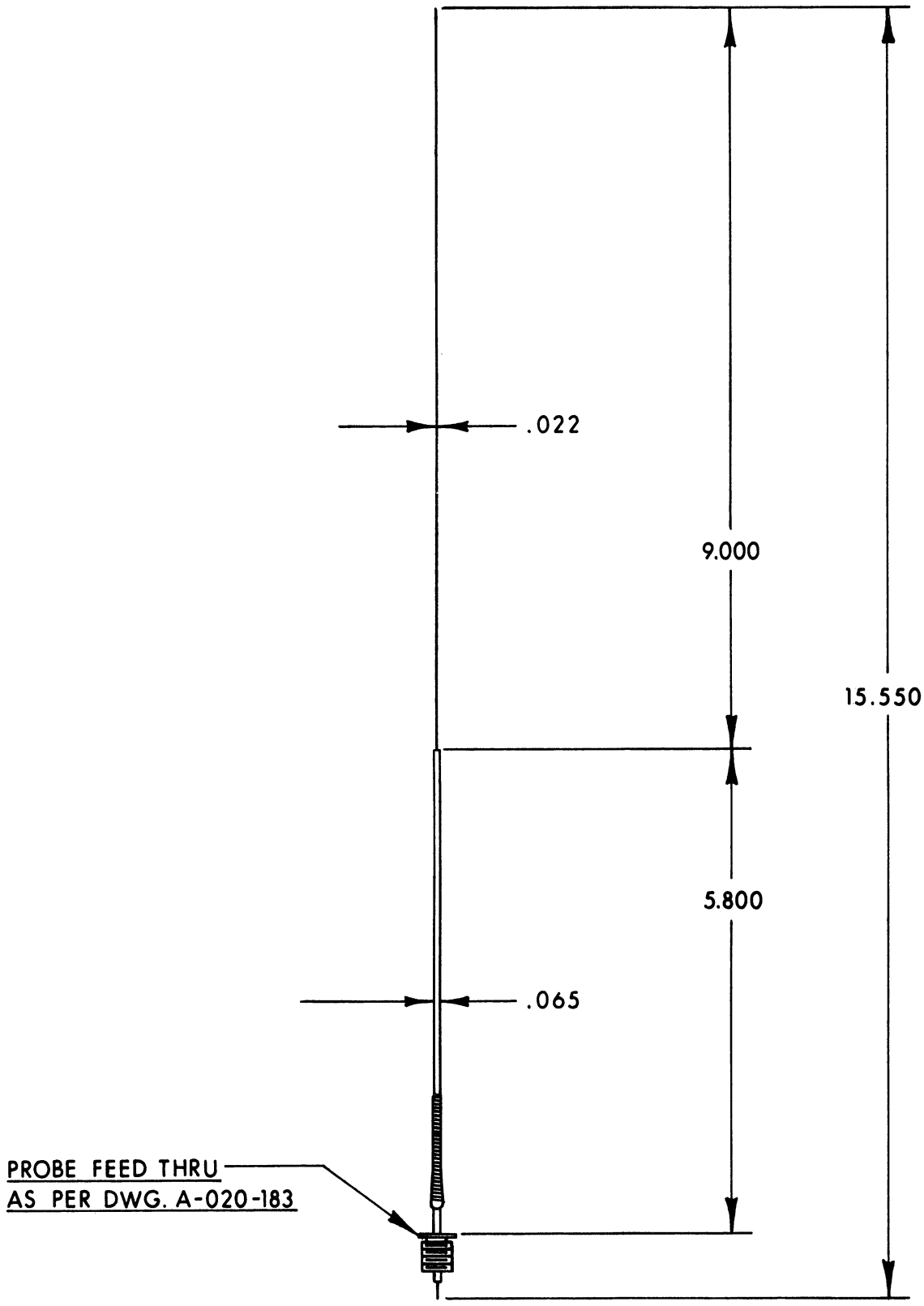

Figure 10. Electron temperature and density probe.

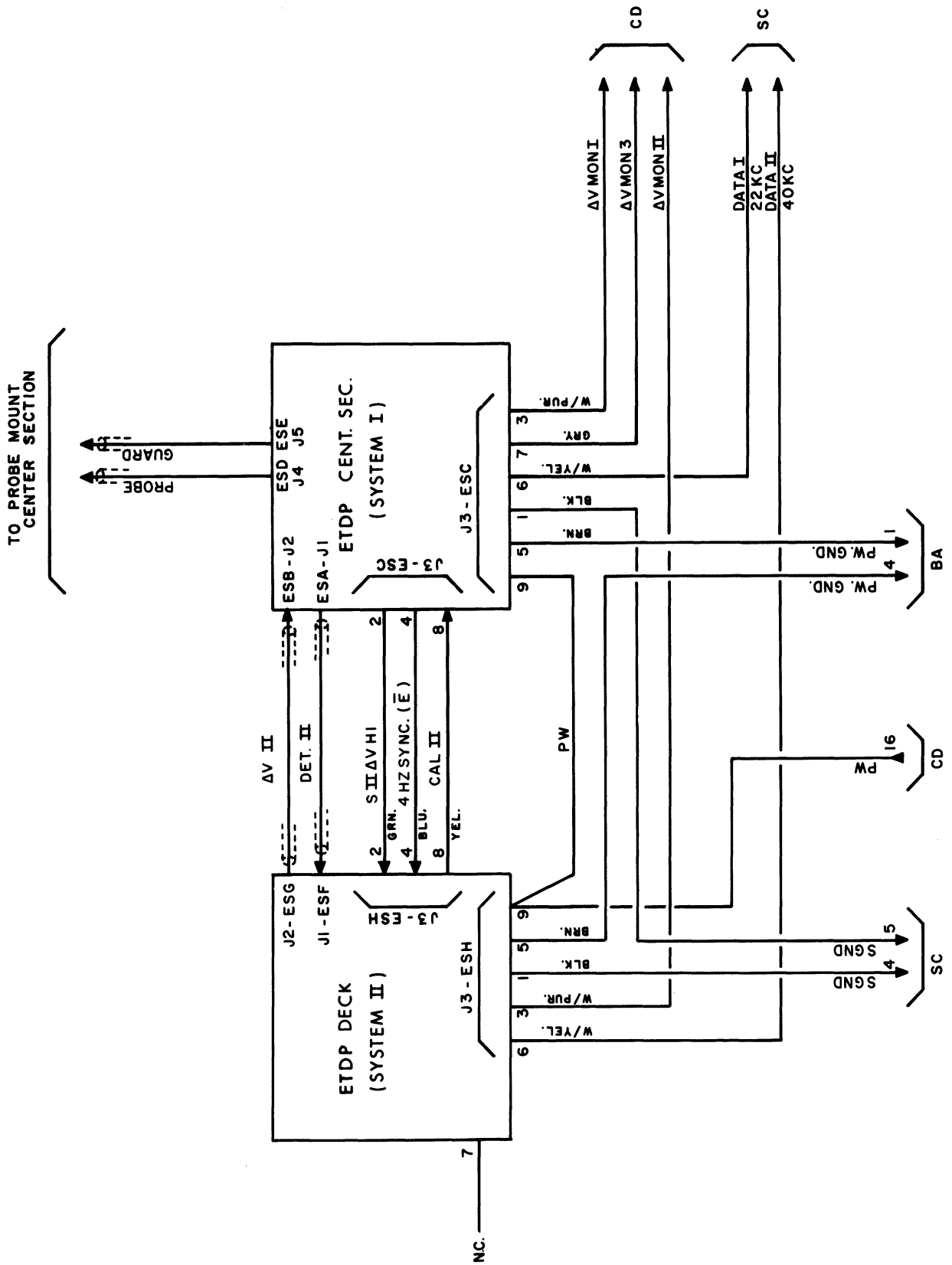

Figure 11. Interconnection of ETDP System I and System II.

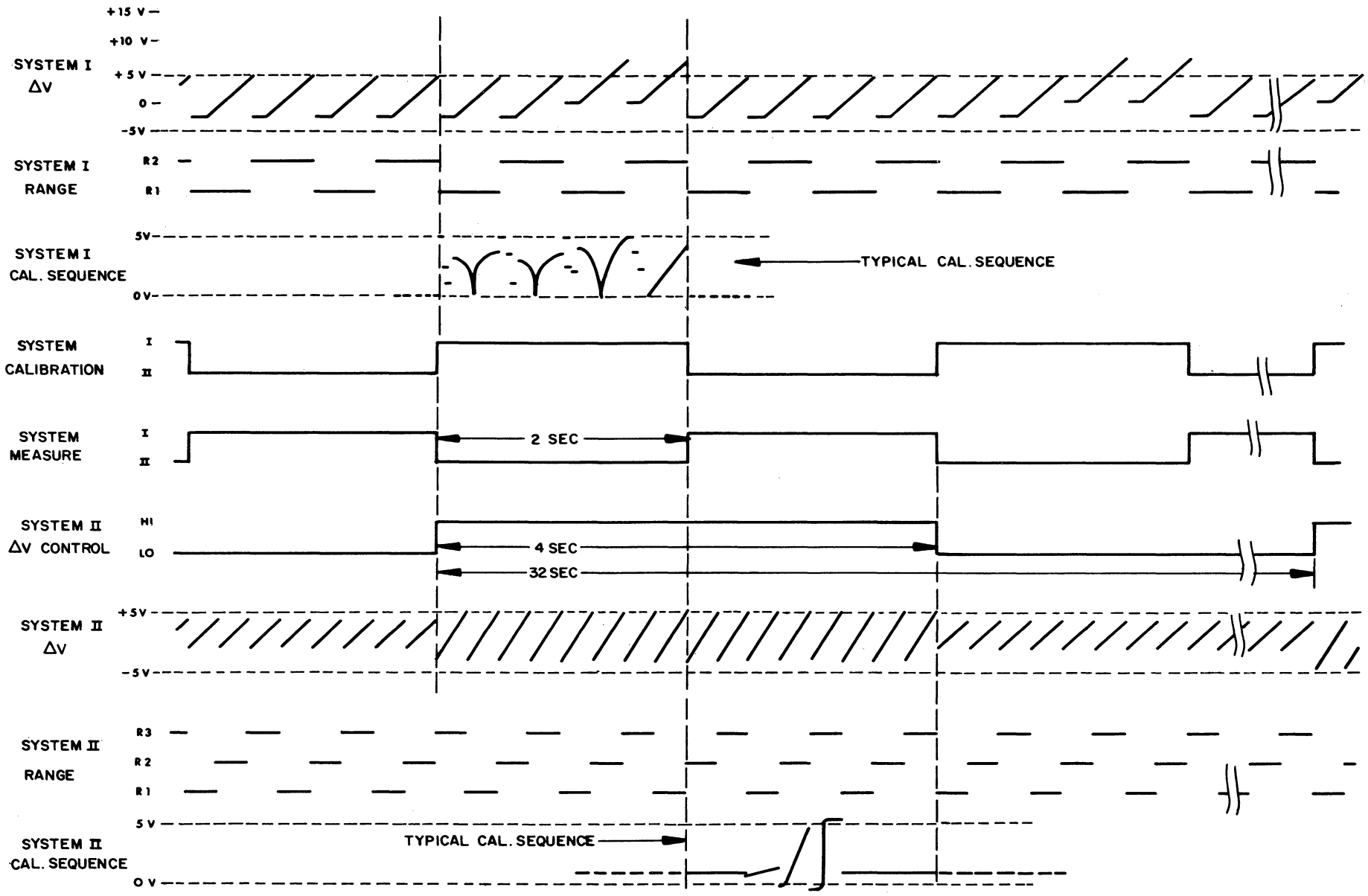

Figure 12. ETDP timing and sequencing.

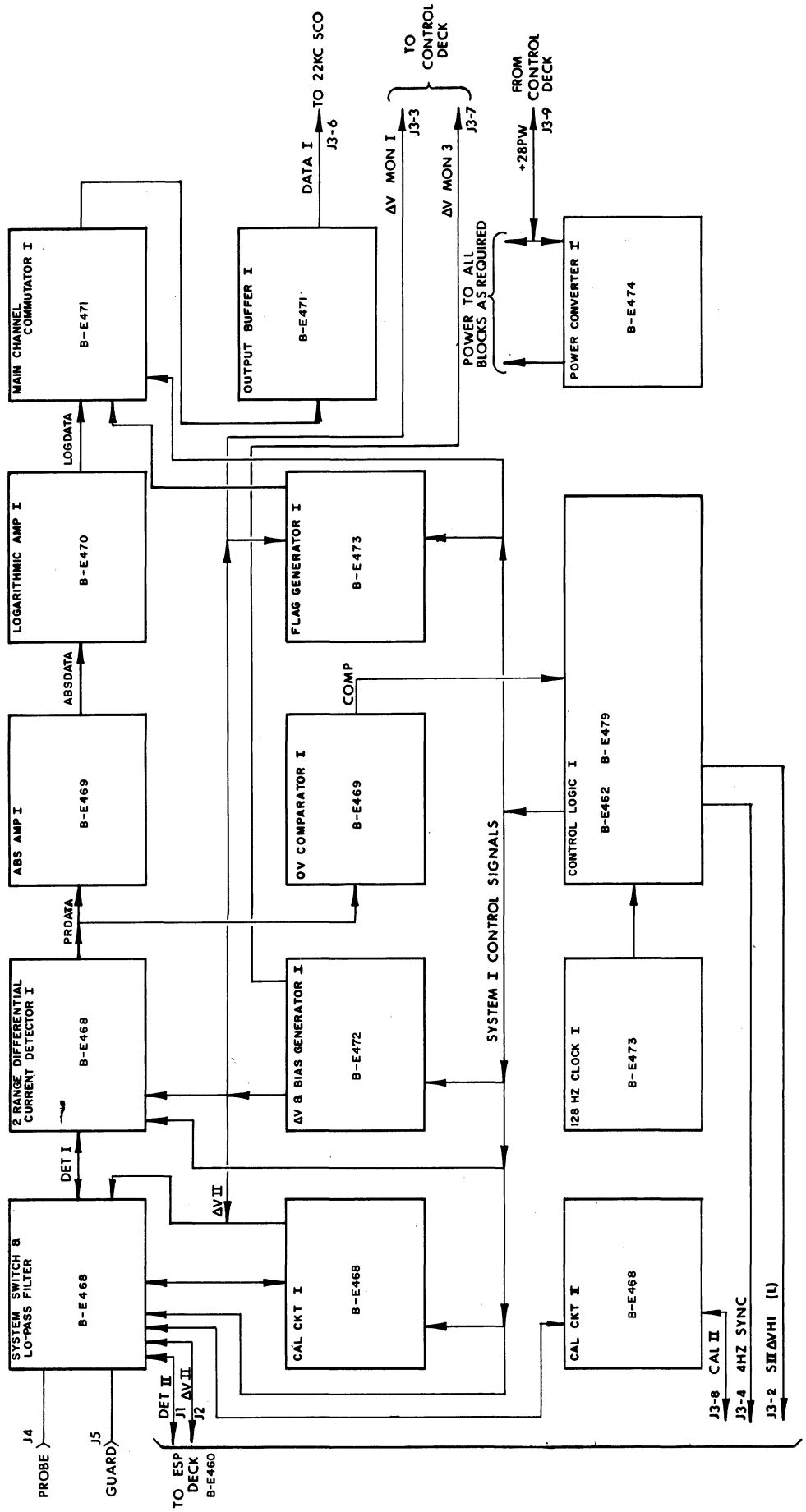

Figure 13. ETDP System I block diagram.

(a) Input Power

1.8 W at 28 V

(b) System Sensitivity

Range 1	0.25 μA full scale (5 V)
Range 2	25 μA full scale (5 V)

(c) Ramp Voltage (ΔV)

Bias Level	from -2.0 to +10.7 V
Ramp Amplitude	-2.5 to +3.5 V from bias point
Slope	14.8 V/sec
Period	408 msec

(The ramp bias level is automatically determined by the vehicle potential at the beginning of each sweep.)

(d) Calibration

System calibration occurs every 4 sec for 2 sec duration. Each calibration sequence consists of a low current calibration for each range, a full scale calibration for one range, and a ΔV sample sweep. The ΔV sample sweep alternates with Range 1 and Range 2 full scale calibrations each calibration sequence (see Figure 12). The ΔV applied to the probe is determined by the transfer function $\Delta V_{app} = 1.35$ (ΔV sample).

(e) Output

Voltage Limits	-0.68 and +5.8 V
Resistance	1600 Ω
Format	A typical output sweep is shown in Figure 14 below.

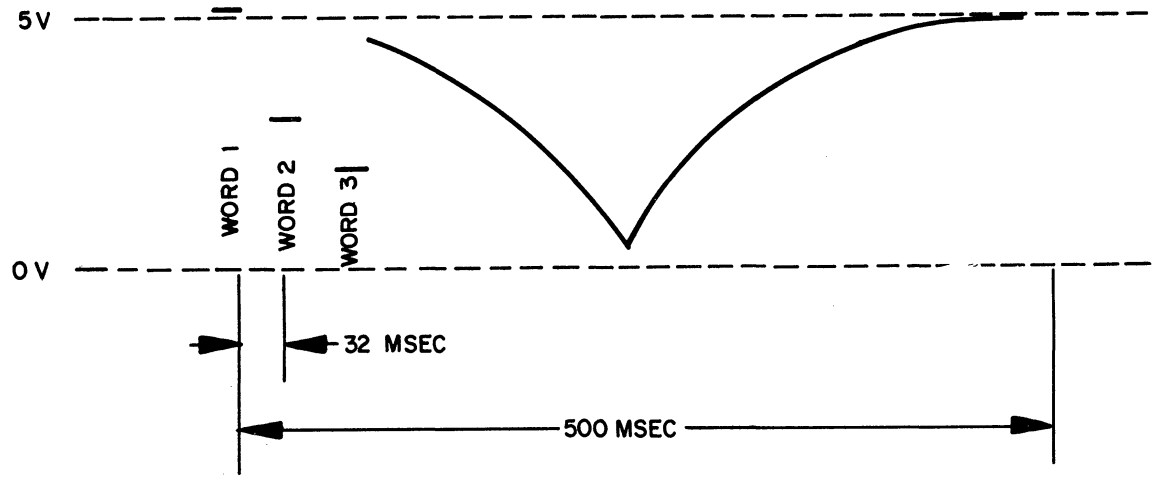

Figure 14. A typical ETDP System I output sweep.

	Function	Voltage	System Function
Analog word 1	Sync	5.1 V	Frame start
Analog word 2	Range and Calibration	0.56 V	Range 1 measure
		1.51 V	Range 2 measure
		2.42 V	Range 1 calibration
		3.38 V	Range 2 calibration
Analog word 3	ΔV Start Voltage	ΔV_{app} start = 2.70 (Word 3) - 4.89 V	

(f) System Transfer Function

$$\text{Range 1} \quad E_o = 2 \log_{10}\left[\frac{|4 \times 10^7 I_p| + .0316}{.0316}\right]$$

$$\text{Range 2} \quad E_o = 2 \log_{10}\left[\frac{|4 \times 10^5 I_p| + .0316}{.0316}\right]$$

where I_p = the current collected by the Langmuir probe.

5.2.2. System II Electronics

The System II electronics unit produces as its output a voltage that is proportional to the current collected by the cylindrical Langmuir probe. This system contains a dc-dc convertor, a ΔV ramp generator, a three range current detector, an in-flight calibration system, and associated control logic and switching devices.

This system also receives a ΔV sync signal from System I to insure that the probe is switched between systems only at the start of a ΔV sweep, and a high-low ΔV control signal which forces the system to high ΔV for 4 out of every 32 sec. The block diagram for System II is shown in Figure 15 and the system specifications are given below:

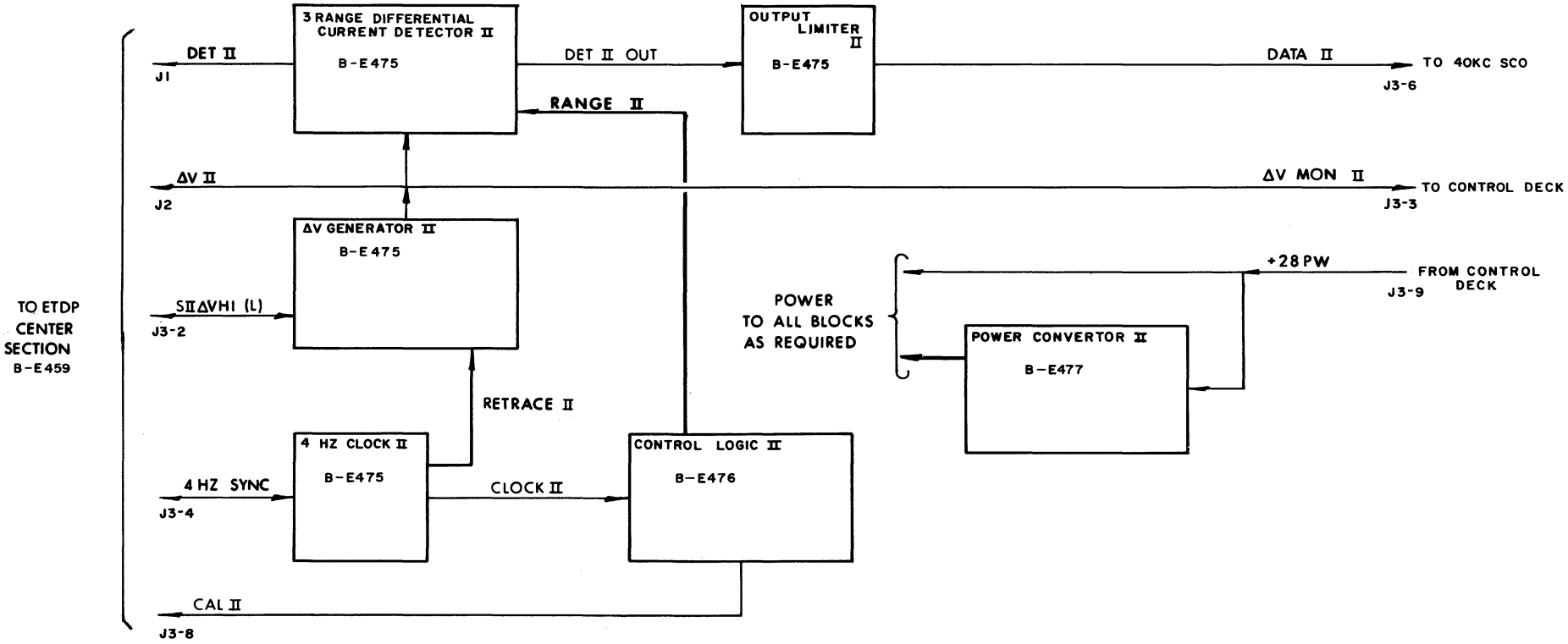

Figure 15. ETDP System II block diagram.

(a) Input Power

1.85 W at 28 V

(b) System Sensitivity

Range 1	10 μA full scale (4 V), 0.4 V/μA
Range 2	1.0 μA full scale (4 V), 4 V/μA
Range 3	0.1 μA full scale (4 V), 40 V/μA

(c) Ramp Voltage (ΔV)

High ΔV	Amplitude -3 to +5 V
	Slope 32 V/sec
Low ΔV	Amplitude -1 to +3 V
	Slope 16 V/sec
Period	250 msec

High-Low ΔV is controlled by System I.

(d) Calibration

Calibration occurs for 2 out of every 4 sec and is controlled by System I. Each calibration sequence contains the common mode checks for ranges 1, 2, and 3 followed by range 1, 2, and 3 calibrations. The order of the calibration sequence is always the same but the starting point may occur at the beginning of any sweep (see Figure 12). A portion of the calibration sequence is always repeated before the system is returned to the measure mode.

(e) Output

Bias Level	0.5 V
Impedance	2000 Ω
Limits	-0.6 to +5.8 V

5.3. SUPPORT MEASUREMENTS AND INSTRUMENTATION

5.3.1. Aspect Determination System

The NASA 18.49 TP utilized a lunar sensor made at SPRL identical to ones used on previous nighttime shots. The system functioned properly throughout the flight and the aspect data were analyzed by the technique which uses the velocity vector as a reference (Taeusch, Carignan, Niemann, and Nagy, 1965). The resulting angle of attack, determined to an estimated accuracy of ±5 deg, is plotted versus altitude in Figure 16.

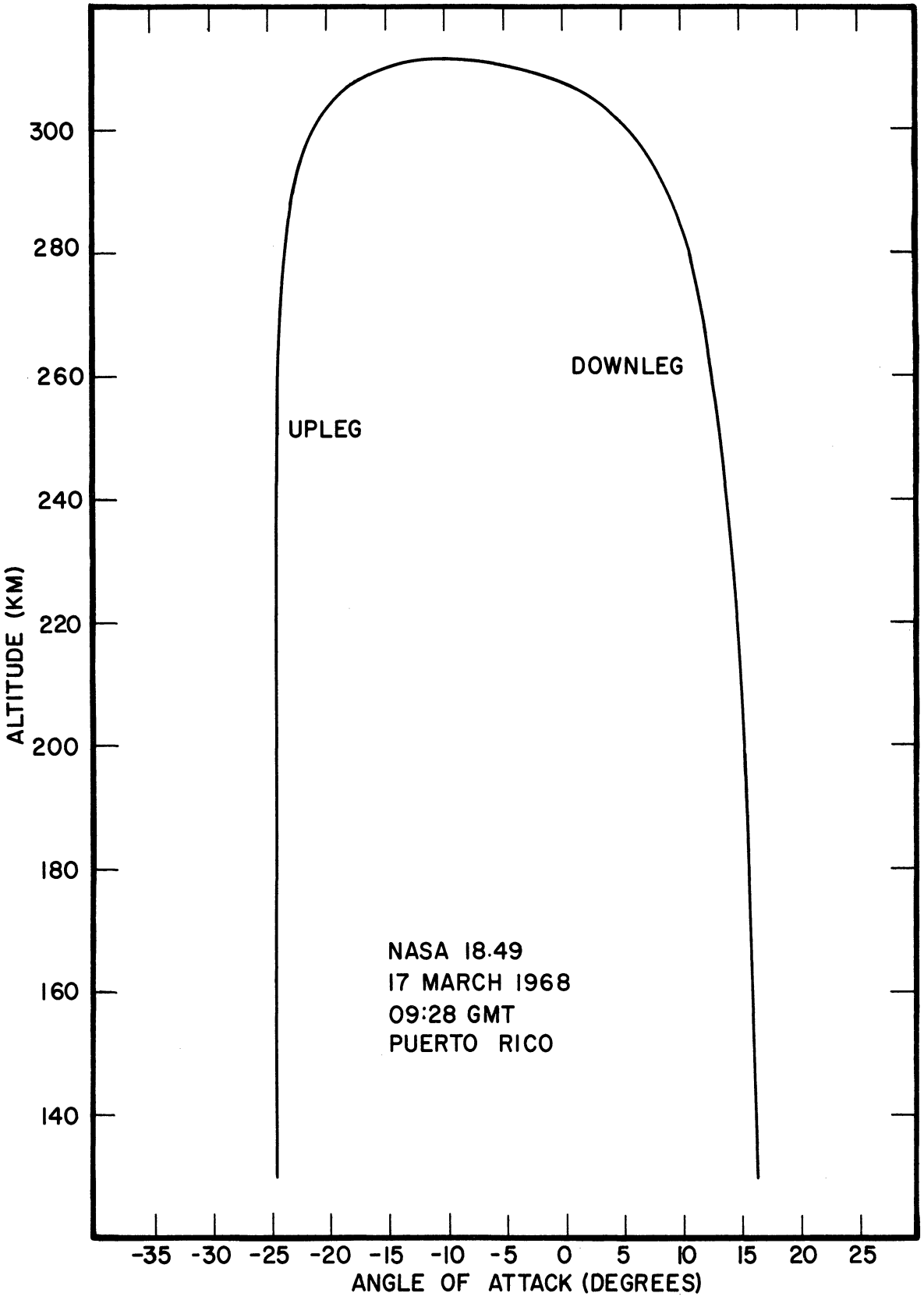

Figure 16. Minimum angle of attack vs. altitude.

5.3.2. Telemetry

The payload data were transmitted in real time by a five channel PAM/FM/FM telemetry system at 240.2 MHz with a nominal output of 2.5 W. The telemetry system used five subcarrier channels, as outlined below.

Transmitter: Driver TRPT-251RBO, Serial No. 2659
Power Amplifier TRFP-2V, Serial No. 482
Mixer Amplifier TA59A, Serial No. 1152
Subcarrier Channels (SCO Type TS58)

IRIG Band	Serial No.	Center Frequency	Function	Low Pass Filter Used
18	3344-25	70 kHz	Omegatron	500 Hz CD
16	3296-25	40 kHz	ESP Data 2 (Old)	330 Hz CD
14	2531-25	22 kHz	ESP Data 1 (New)	330 Hz CD
12	3202-25	10.5 kHz	Aspect	450 Hz CA
11	1684-5	7.35 kHz	Commutator	160 Hz CD

Instrumentation power requirements totalled approximately 30 W, supplied by a Yardney HR-1 Silvercell battery pack of a nominal 28 V output.

5.3.3. Housekeeping Monitors

Outputs from various monitors throughout the instrumentation provided information bearing on the operations of the electronic components during flight. These outputs were fed to a thirty-segment commutator which ran at one rps. The commutator assignments were as follows:

COMMUTATOR FORMAT FOR NASA 18.49

Segment Number	Segment Assignment
1	Amplifier Range
2	Omegatron Output
3	Filament Monitor
4	Emission Current Monitor
5	Bias Voltage Monitor
6	RF Voltage Monitor
7	Internal Pressure Monitor
8	Thermistor-Gauge Temperature
9	Thermistor-Amplifier Temperature
10	Thermistor-Filament Regulator Temperature
11	Thermistor-Oscillator Temperature
12	Thermistor-Transmitter Temperature
13	Thermistor-Commutator Temperature
14	Battery Voltage Monitor
15	Ledex Position Monitor
16	Omegatron Output
17	Omegatron Output
18	Omegatron Output
19	Omegatron Output
20	Omegatron Output
21	Omegatron Output
22	Omegatron Output
23	Omegatron Output
24	0 V Calibration
25	1 V Calibration
26	2 V Calibration
27	3 V Calibration
28	4 V Calibration
29	5 V Calibration
30	5 V Calibration

6. ANALYSIS OF DATA

The telemetered data were recorded at the launch site by a mobile telemetry receiving station. Appropriate paper records were made from the magnetic masters, facilitating "quick look" evaluations. The aspect data were reduced to engineering parameters from paper records. The omegatron and housekeeping data were reduced by computer techniques from the magnetic tapes.

6.1. TRAJECTORY AND ASPECT

The position and velocity data used to determine aspect, ambient N_2 density, and ambient temperature as a function of time and altitude were obtained by fitting a smooth theoretical trajectory to the rather minimal MPS-19 radar data. Positional data were received from the radar for two brief segments of flight time: from 6 to 27 sec, and from 53 to 90 sec. "Fair to poor" velocity data were derived from the slight positional data for the interval of 57 to 88 sec. This information, however, was sufficient to establish a trajectory. The theoretical trajectory is programmed for computer solution similar to that described by Parker (1962). The analysis of minimum angle of attack (α_{min}) as described by Carter (1968) is also incorporated in the program. The output of the computer furnishes α_{min}, altitude, and velocity as a function of time. A plot of α_{min} versus altitude has already been given in Figure 16. Figure 17 shows the occurrence of significant events during the flight.

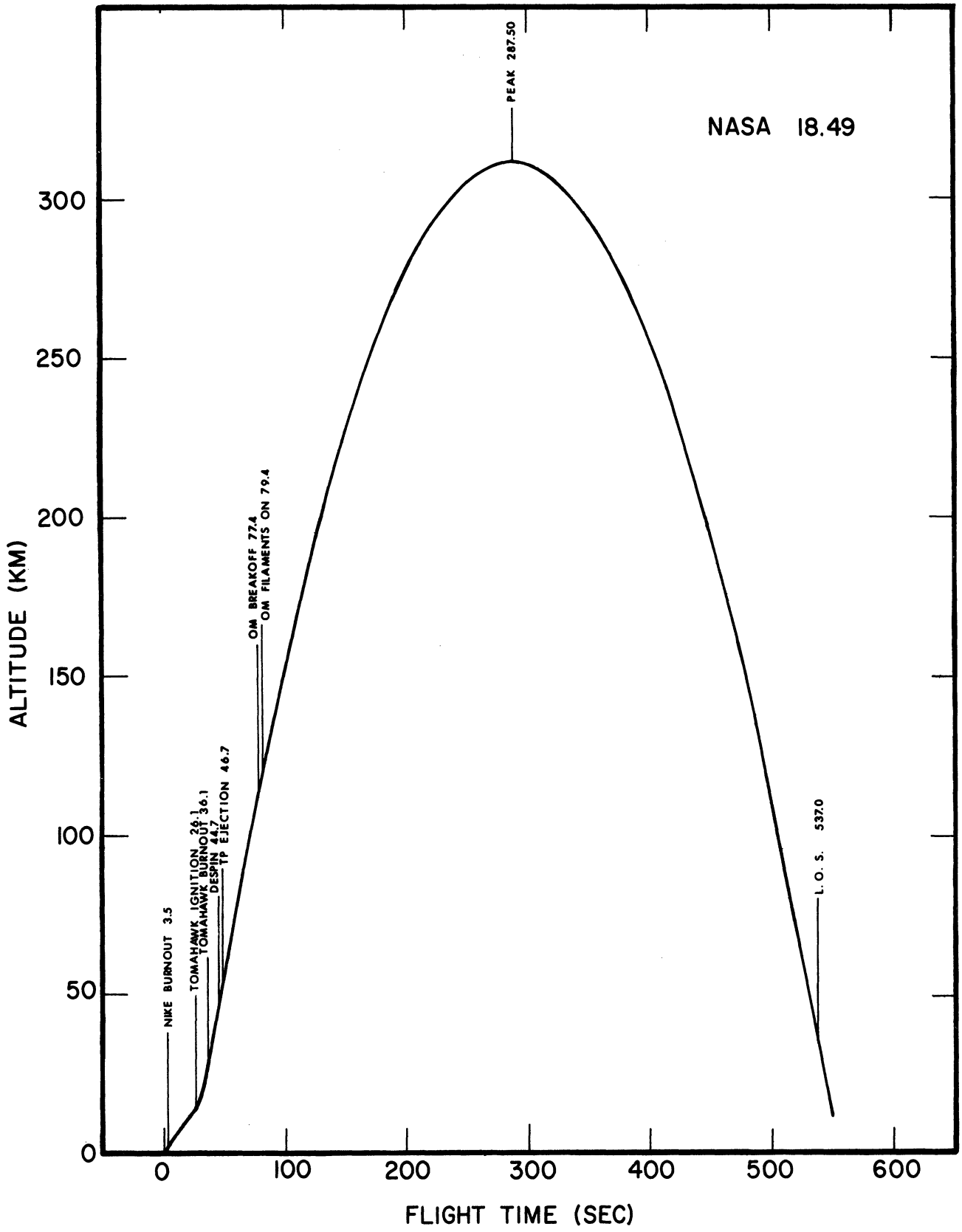

Figure 17. Sequence of events.

6.2. AMBIENT N_2 DENSITY

The neutral molecular nitrogen density was determined from the measured gauge partial pressure as described by Spencer, et al., (1965, 1966), using the basic relationship:

$$n_a = \left(\frac{\Delta n_i u_i}{2\sqrt{\pi}\ V \cos \alpha_{min}} \right) K(S_o, \alpha)$$

where

n_a = ambient N_2 number density
Δn_i = maximum minus minimum gauge number density during one tumble, A x ΔI, where A is the sensitivity of the gauge
u_i = $\sqrt{2kT_i/m}$, most probable thermal speed of particles inside gauge
T_i = gauge wall temperature
V = vehicle velocity with respect to the earth
α_{min} = minimum angle of attack for one tumble
$K(S_o, \alpha)$ = the reciprocal of the normalized transmission probability as defined by Ballance (1967), referred to as the geometry correction factor.

ΔI, the difference between the maximum (peak) omegatron gauge current and the minimum (background) gauge current versus flight time is shown in Figure 18. The background current is the result of the outgassing of the gauge walls, and the inside density is due to atmospheric particles which have enough translational energy to overtake the payload and enter the gauge. The outgassing component is assumed constant for one tumble and affects both the peak reading and the background reading, and, therefore, does not affect the difference. From calibration data obtained by standard techniques, the inside number density, Δn_i, is computed for the measured current.

By using the measured gauge wall temperature, the most probable thermal speed of the particles inside the gauge, u_i, is computed. The uncertainty in this measurement is believed to be about $\pm$2% absolute.

V, the vehicle velocity with respect to the earth, is obtained from the trajectory curve fitting described previously and is believed to be better than $\pm$1% absolute.

Cos α_{min} is obtained from the aspect analysis described by Carter (1968). Since the uncertainty in cos α_{min} depends upon α_{min}, for any given uncertainty in α_{min}, each particular case and altitude range must be considered separately. Figure 16 shows that the minimum angle of attack for the downleg is generally about fifteen degrees, so with an assumed maximum uncertainty in α_{min} of $\pm$5 degrees, the resulting uncertainty in cos α_{min} is less than $\pm$3%. The data for low angle of attack were used as control data.

$K(S_o,\alpha)$, the geometry correction factor versus altitude, is shown in Figure 19. As can be seen, the maximum correction for OM I is about 6%, or $K(S_o,\alpha) = .94$ at about 140 km altitude for the upleg data. The correction factor, determined from empirical and theoretical studies, is believed known to better than 2%.

The resulting ambient N_2 number density, obtained from the measured quantities described above, is shown in Figure 20 and is tabulated in Table III. The uncertainty in the ambient density due to the combined uncertainties in the measured quantities is thought to be 10% relative and 25% absolute.

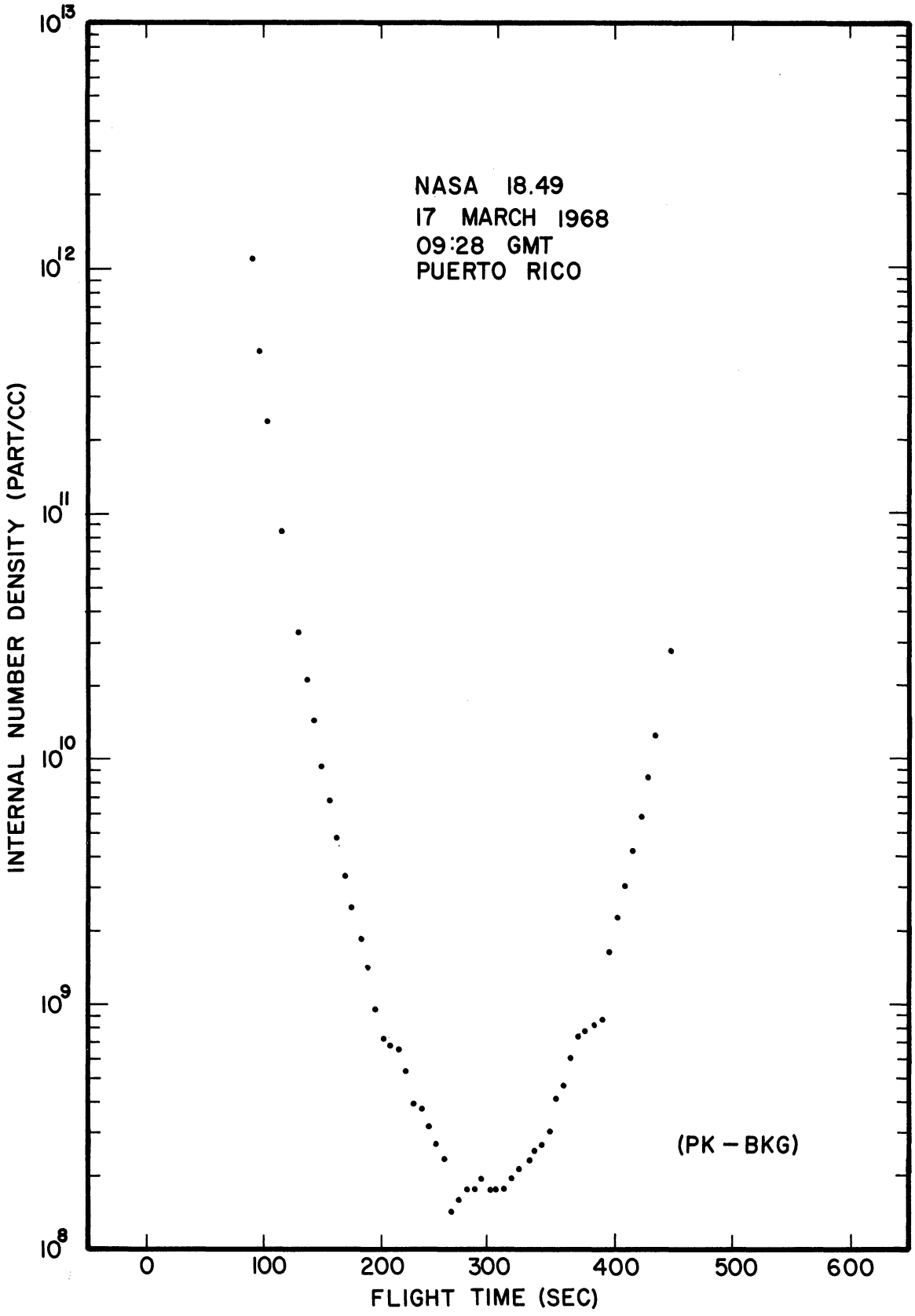

Figure 18. Omegatron current vs. flight time.

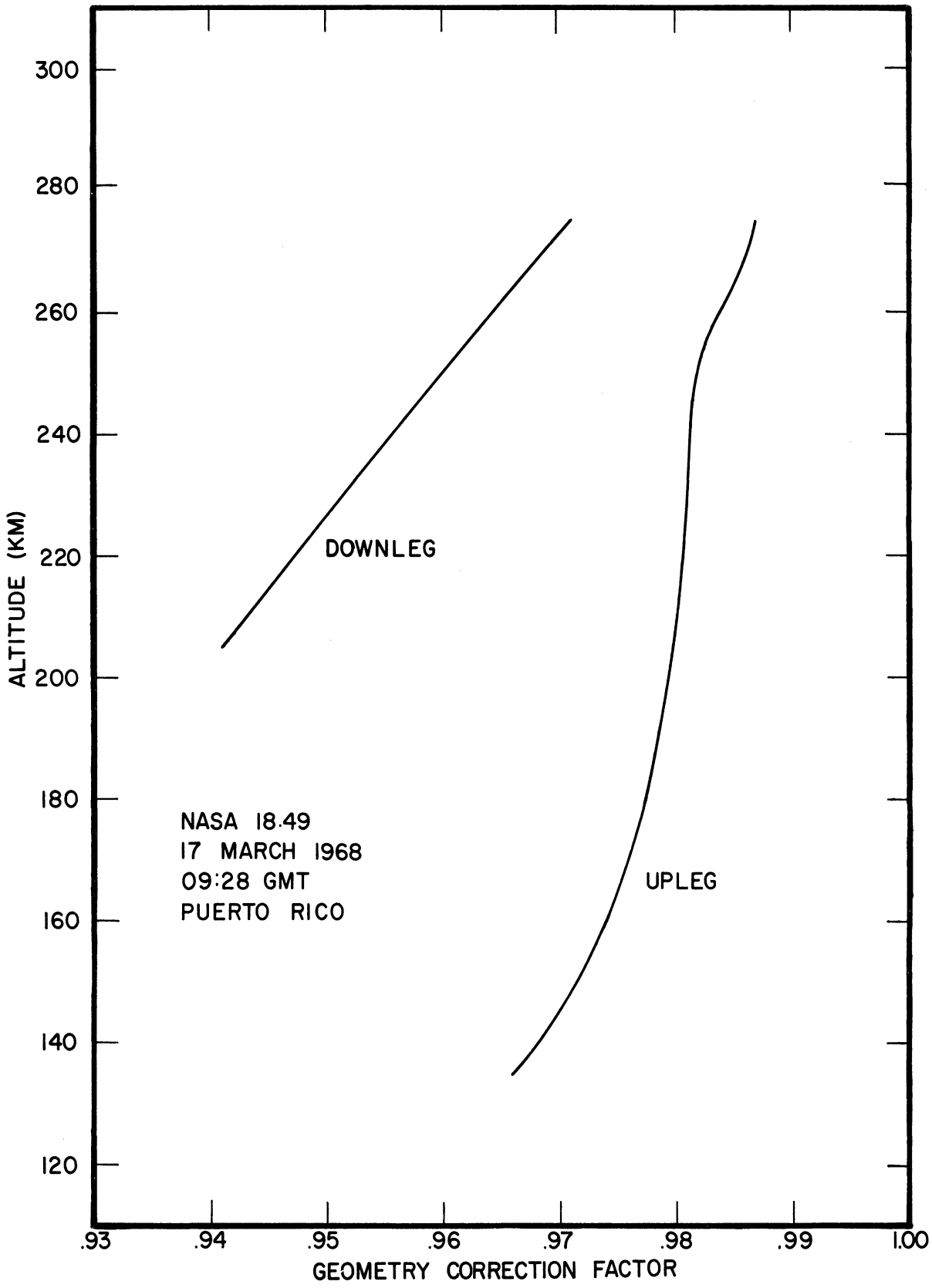

Figure 19. $K(S_o, \alpha)$ vs. altitude.

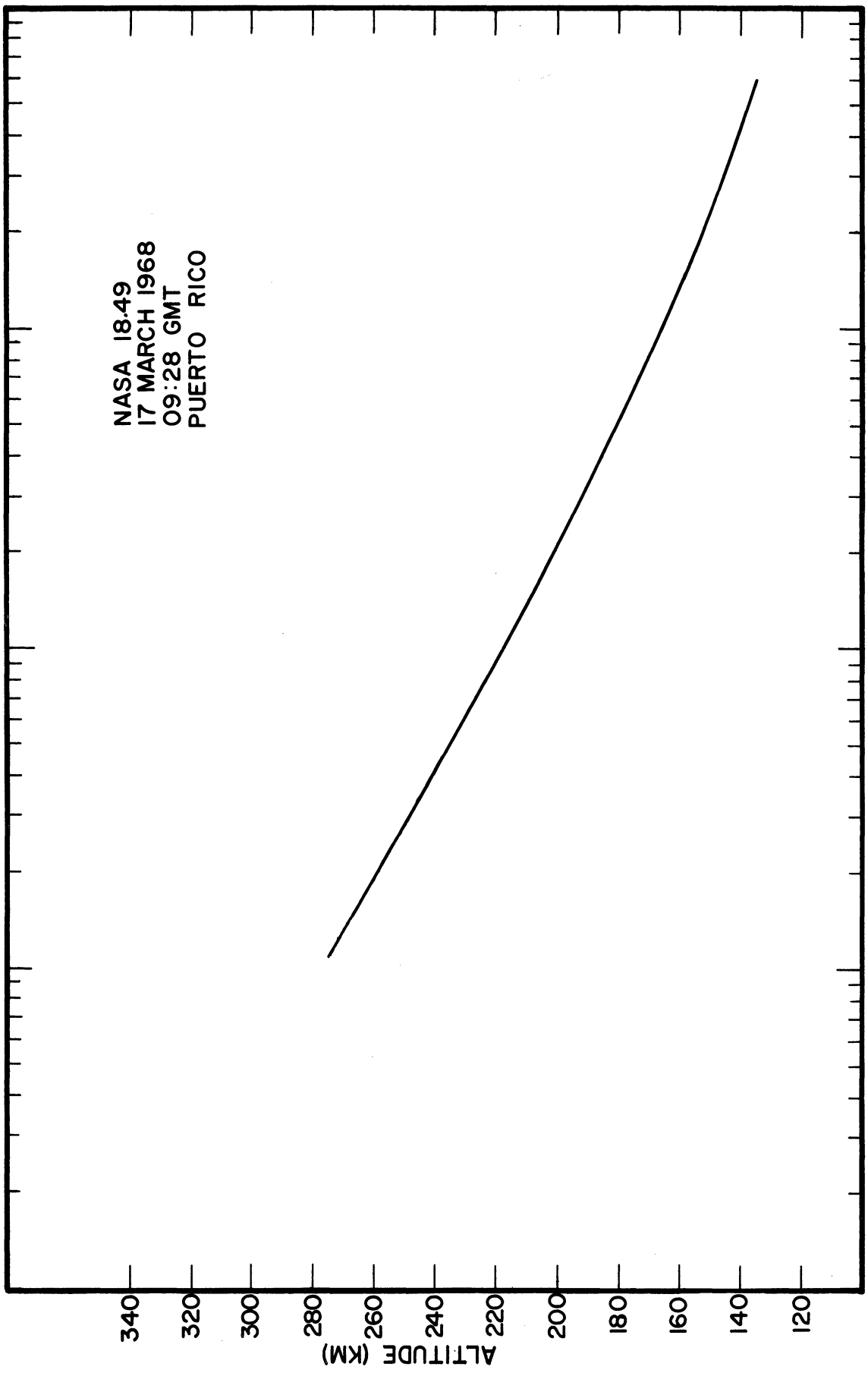

Figure 20. Ambient N_2 density vs. altitude.

TABLE III

N_2 AMBIENT DENSITY DATA

NASA 18.49
17 March 1968
09:28 GMT
05:28 Local
Puerto Rico

Altitude (km)	Temperature (°K)	Density (part/cc)
135	550	5.87×10^{10}
140	581	4.21
145	608	3.08
150	634	2.29
155	657	1.74
160	676	1.33
165	692	1.03×10^{10}
170	704	8.09×10^{9}
175	717	6.37
180	728	5.06
185	737	4.04
190	745	3.24
195	753	2.60
200	760	2.10
205	767	1.69
210	773	1.37
215	779	1.12×10^{9}
220	785	9.10×10^{8}
225	790	7.44
230	796	6.09
235	800	4.99
240	804	4.10
245	807	3.38
250	810	2.78
255	812	2.30
260	814	1.90
265	815	1.58
270	816	1.31
275	817	1.09×10^{8}

Fit Parameters: $T_\infty = 827°K$
$T_o = 554°K$
$P_b = 9.15 \times 10^{-9}$ torr
$\sigma = 2.23 \times 10^{-2}$

6.3. TEMPERATURE

The ambient temperature profile shown in Figure 21, tabulated in Table III, was obtained by integrating the measured N_2 density profile to obtain a partial pressure profile and by relating the known density and pressure to the temperature through the ideal gas law. In this procedure, the assumptions of hydrostatic equilibrium and perfect gas behavior are implicit. It can be shown that the density integral is stable and highly convergent if carried out in the direction of increasing density. Since the density is finite at the initial boundary of integration, it is necessary to determine an initial pressure or temperature in order for the temperature results to be immediately meaningful. In the past, this boundary temperature was chosen intuitively. In an effort to eliminate this rather arbitrary choice, the following technique for determining a boundary pressure was implemented.

Assuming hydrostatic equilibrium and ideal gas behavior, we know that

$$\frac{dP_i}{dH} = - n_i m_i g_o \qquad (6.3.1)$$

and

$$P_i = n_i k T_i \ , \qquad (6.3.2)$$

where

g_o = sea level acceleration due to gravity,
H = geopotential altitude = $R_o Z/(R_o + Z)$,
k = Boltzmann's constant,
m_i = molecular mass of constituent i,
n_i = the number density of constituent i (in our case N_2),
P_i = partial pressure of constituent i,
R_o = radius of the earth (6356.77 km),
T_i = kinetic temperature of constituent i,
Z = geometric altitude.

Integrating Equation (6.3.1) in the direction of increasing density,

$$P_i(H) = P_{i_b} - g_o m_i \int_{H_b}^{H} n(H)dH \qquad (6.3.3)$$

where

H_b = geopotential altitude of the boundary whose geometric altitude is Z_b,

P_{i_b} = partial pressure at the boundary.

Dropping the subscript and noting that we are dealing with single known constituents, the above integral may be approximated numerically by

$$P(Z_i) = P_b + g_o R_o^2 m \sum_{j=1}^{i} \frac{(Z_{j-1} - Z_j)(n_{j-1} - n_j)}{(R_o + Z_{j-1})(R_o + Z_j)(\ell n\, n_{j-1} - \ell n\, n_j)} \tag{6.3.4}$$

where the subscript j is assigned to the data in the order of increasing n (i.e., j = 1 at highest altitude of the data set n(Z)).

Combining Equations (6.3.2) and (6.3.4) to obtain temperature,

$$T(Z_i) = \frac{P(Z_i)}{kn(Z_i)} \quad . \tag{6.3.5}$$

It is readily apparent that for any given density profile there are an infinite number of solutions to Equation (6.3.5), one solution for each P_b or T_b chosen.

It has been found that a suitable value for P_b may be determined by means of a least squares fitting procedure using a fitting function based on the empirical expression for the temperature profile given by Jacchia (1964). This expression may be written, as suggested by Walker (1965),

$$T(H) = T_\infty - (T_\infty - T_o) \exp[-\sigma H] \tag{6.3.6}$$

where

T_∞ = exospheric temperature

T_o = reference temperature

σ = a shape factor.

The difference between the temperature profile given by (6.3.5) and (6.3.6) is

$$\varepsilon(Z_i) = T_\infty - (T_\infty - T_o) \exp\left[-\sigma\left(\frac{R_o Z_i}{R_o + Z_i}\right)\right] - \frac{P(Z_i)}{kn(Z_i)} \quad . \tag{6.3.7}$$

Using the general least squares approach we must minimize

$$Q = \sum_{i=1}^{\ell} [\varepsilon(Z_i)]^2 \qquad (6.3.8)$$

where ℓ is the number of data points representing the density profile. Q is minimum when

$$\frac{\partial Q}{\partial T_\infty} = \frac{\partial Q}{\partial T_o} = \frac{\partial Q}{\partial P_b} = 0$$

and

$$\frac{\partial Q}{\partial \sigma} = 0 \ . \qquad (6.3.9)$$

The first part of Equation (6.3.9) yields a set of three linear equations which are readily solved and give values for T_∞, T_o, P_b, and Q for any given value of σ. Choosing several appropriate values for σ leads to a solution of the last of Equation (6.3.9), i.e., $\partial Q/\partial \sigma = 0$. Having the value of σ which minimizes Q, the first part of Equation (6.3.9) may be solved again, thus providing T_∞, T_o, P_b for the best least squares fit to Equation (6.3.6).

Utilizing the P_b determined above, Equation (6.3.5) may be solved for $T(Z_i)$.

The values of the fitting parameters obtained for these data are given in Table III. T_∞ is the apparent exospheric temperature for these data.

6.4. GEOPHYSICAL INDICES

The 10.7 cm solar flux ($F_{10.7}$) and the geomagnetic activity indices (a_p) for the appropriate periods are shown in Figures 22 and 23.

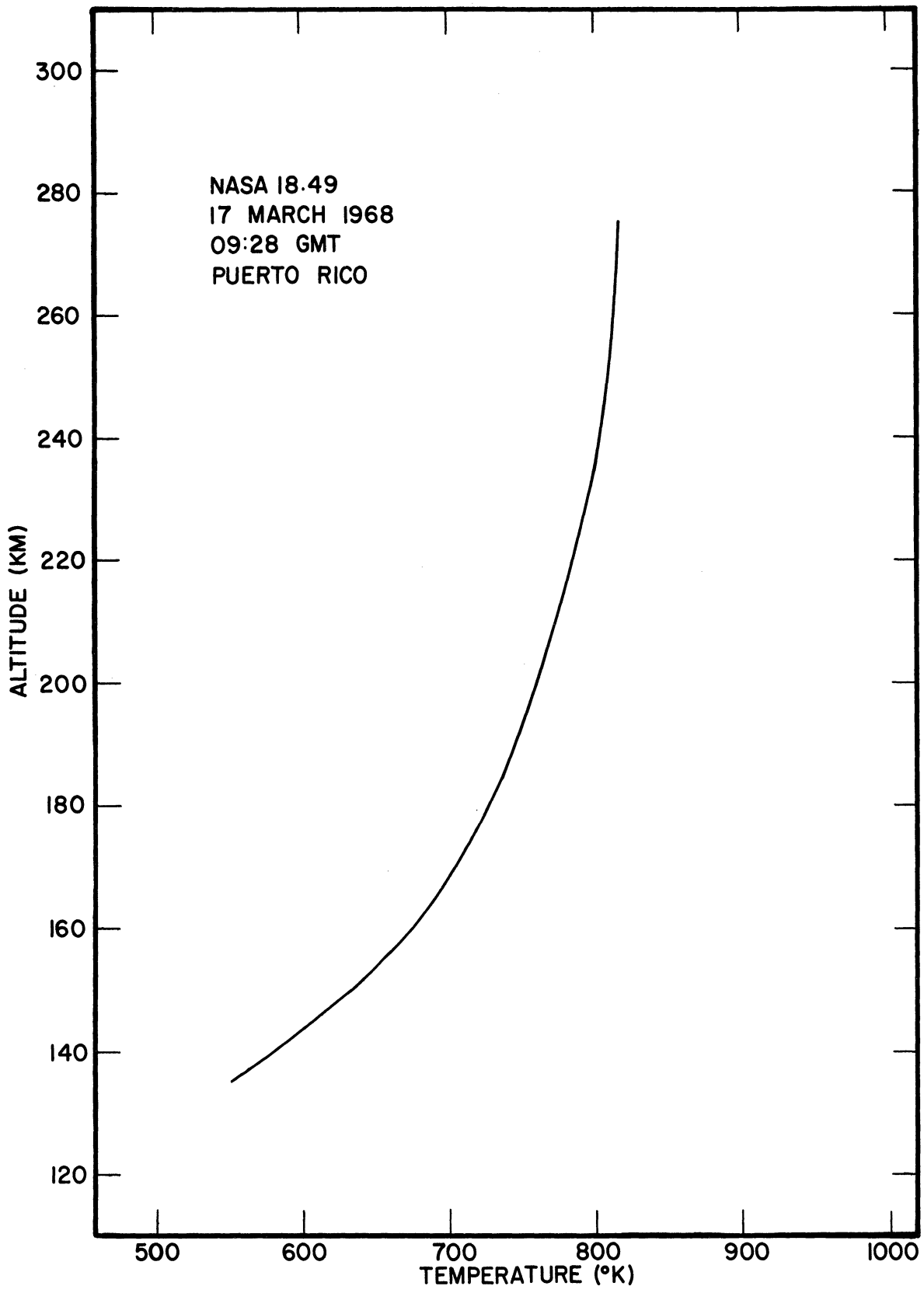

Figure 21. Neutral particle temperature vs. altitude.

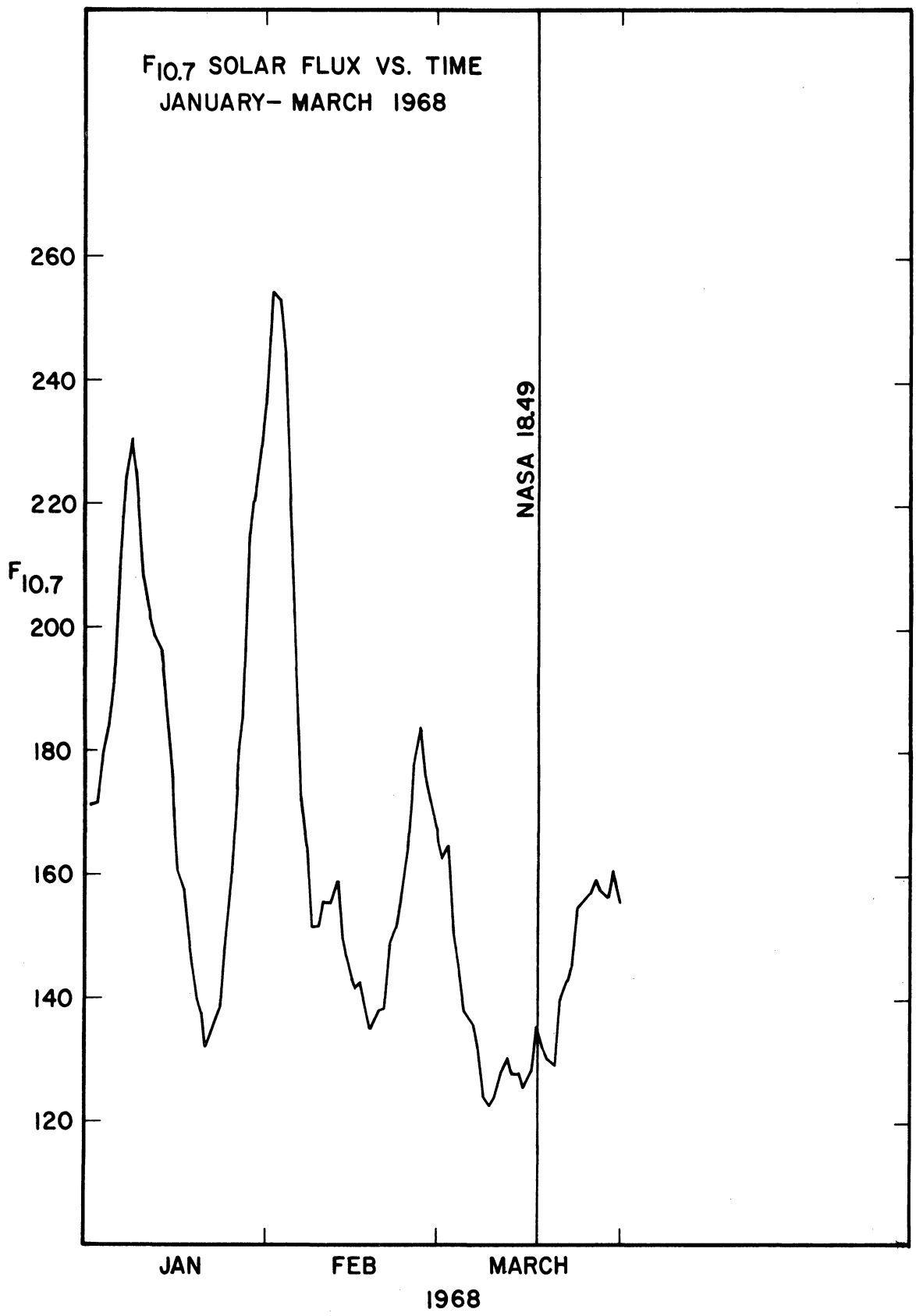

Figure 22. Solar flux at 10.7 cm wavelength.

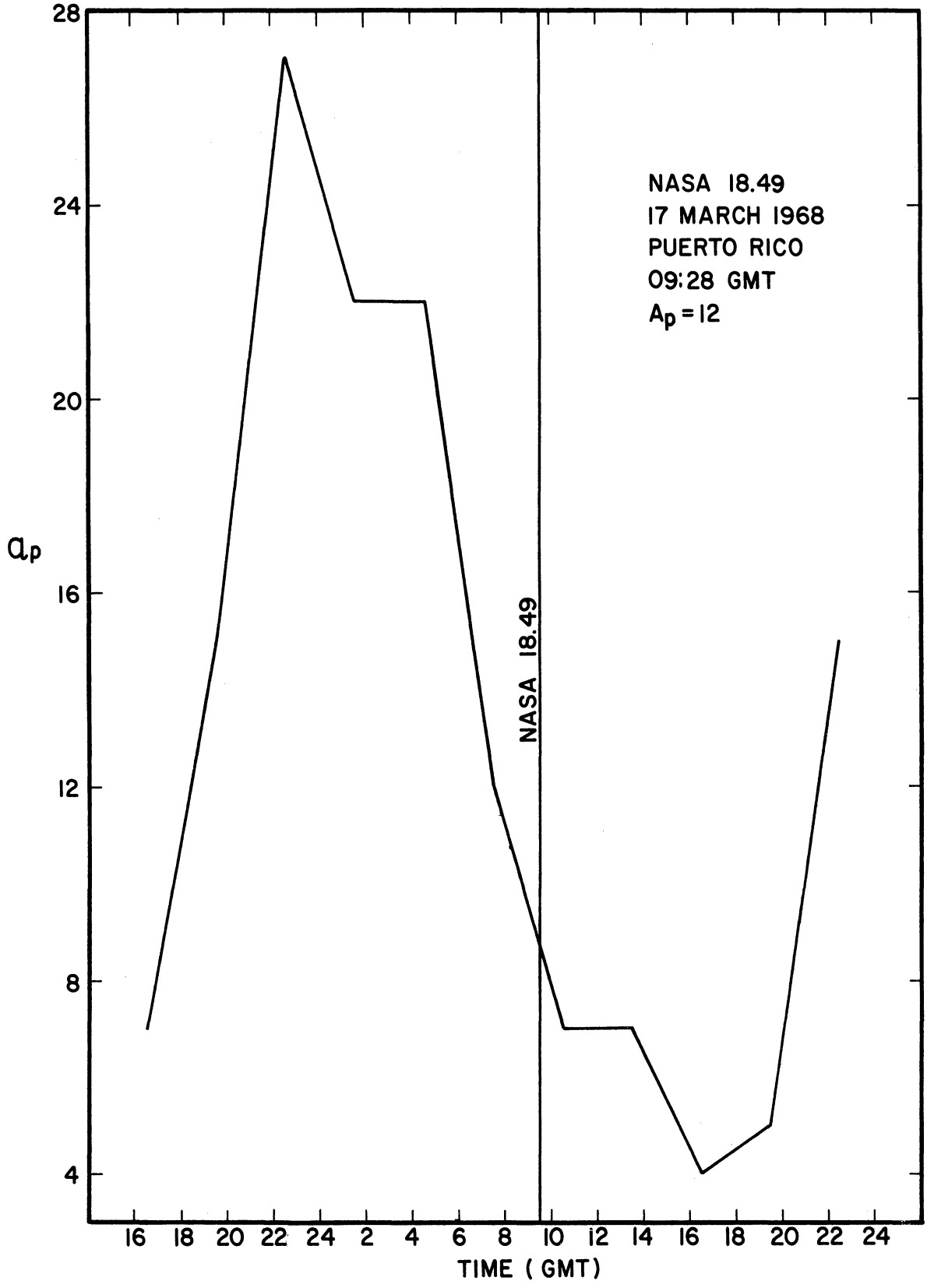

Figure 23. Three-hour geomagnetic activity index (a_p).

7. REFERENCES

Ballance, James O., An Analysis of the Molecular Kinetics of the Thermosphere Probe, George C. Marshall Space Flight Center, NASA Technical Memorandum, NASA TM X-53641, July 31, 1967.

Carter, M. F., The Attitude of the Thermosphere Probe, University of Michigan Scientific Report 07065-4-S, April 1968.

Jacchia, L. G., Static Diffusion Models of the Upper Atmosphere with Empirical Temperature Profiles, Research in Space Science, Smithsonian Astrophysical Observatory Special Report No. 170, 1964.

Niemann, H. B. and Kennedy, B. C., "An Omegatron Mass Spectrometer for Partial Pressure Measurements in Upper Atmosphere," Review of Scientific Instruments, 37, No. 6, 722, 1966.

Parker, L. T., Jr., A Mass Point Trajectory Program for the DCD 1604 Computer, Technical Document Report AFSW-TDR-49, Air Force Special Weapons Center, Kirtland Air Force Base, New Mexico, August 1962.

Spencer, N. W., Brace, L. H., and Carignan, G. R., "Electron Temperature Evidence for Nonthermal Equilibrium in the Ionosphere," Journal of Geophysical Research, 67, 151-175, 1962.

Spencer, N. W., Brace, L. H., Carignan, G. R., Taeusch, D. R., and Niemann, H. B., "Electron and Molecular Nitrogen Temperature and Density in the Thermosphere," Journal of Geophysical Research, 70, 2665-2698, 1965.

Spencer, N. W., Taeusch, D. R., and Carignan, G. R., N_2 Temperature and Density Data for the 150 to 300 Km Region and Their Implications, Goddard Space Flight Center, NASA Technical Note X-620-66-5, December 1965.

Taeusch, D. R., Carignan, G. R., Niemann, H. B., and Nagy, A. F., The Thermosphere Probe Experiment, University of Michigan Rocket Report 07065-1-S, March 1965.

Walker, J. C. G., "Analytic Representation of Upper Atmosphere Densities Based on Jacchia's Static Diffusion Models," Journal of Atmospheric Sciences, 22, No. 4, 462-463, July 1965.